The Pattern of Distribution of Amino Groups Modulates the Structure and Dynamics of Natural Aminoglycosides: Implications for RNA Recognition

ARTICLE *in* JOURNAL OF THE AMERICAN CHEMICAL SOCIETY · APRIL 2007

Impact Factor: 12.11 · DOI: 10.1021/ja066348x · Source: PubMed

8 AUTHORS, INCLUDING:

Francisco Corzana
Universidad de La Rioja (Spain)
82 PUBLICATIONS **1,101** CITATIONS
SEE PROFILE

Julia Revuelta
Spanish National Research Council
43 PUBLICATIONS **586** CITATIONS
SEE PROFILE

Jesús Jiménez-Barbero
Center for Cooperative Research in Biosciences
541 PUBLICATIONS **10,253** CITATIONS
SEE PROFILE

Juan Luis Asensio
Spanish National Research Council
102 PUBLICATIONS **2,464** CITATIONS
SEE PROFILE

J|A|C|S
ARTICLES
Published on Web 02/14/2007

The Pattern of Distribution of Amino Groups Modulates the Structure and Dynamics of Natural Aminoglycosides: Implications for RNA Recognition

Francisco Corzana,[†,⊥] Igor Cuesta,[†] Felix Freire,[†] Julia Revuelta,[†] Mario Torrado,[†] Agatha Bastida,[†] Jesús Jiménez-Barbero,[‡] and Juan Luis Asensio*[,†]

Contribution from the Instituto de Química Orgánica General and Centro de Investigaciones Biológicas (CSIC), Juan de la Cierva 3, 28006 Madrid, Spain

Received September 1, 2006; E-mail: iqoa110@iqog.csic.es

Abstract: Aminoglycosides are clinically relevant antibiotics that participate in a large variety of molecular recognition processes involving different RNA and protein receptors. The 3-D structures of these policationic oligosaccharides play a key role in RNA binding and therefore determine their biological activity. Herein, we show that the particular NH_2/NH_3^+/OH distribution within the antibiotic scaffold modulates the oligosaccharide conformation and flexibility. In particular, those polar groups flanking the glycosidic linkages have a significant influence on the antibiotic structure. A careful NMR/theoretical analysis of different natural aminoglycosides, their fragments, and synthetic derivatives proves that both hydrogen bonding and charge−charge repulsive interactions are at the origin of this effect. Current strategies to obtain new aminoglycoside derivatives are mainly focused on the optimization of the direct ligand/receptor contacts. Our results strongly suggest that the particular location of the NH_2/NH_3^+/OH groups within the antibiotics can also modulate their RNA binding properties by affecting the conformational preferences and inherent flexibility of these drugs. This fact should also be carefully considered in the design of new antibiotics with improved activity.

Introduction

Aminoglycosides are highly potent, wide-spectrum bactericidals.[1] These antibiotics participate in a large variety of biologically relevant molecular recognition processes involving both RNA and protein receptors.[2−6] Thus, aminoglycosides bind to the decoding region aminoacyl-tRNA site (A-site) inducing codon misreading and inhibiting translocation, eventually resulting in cell death.[7−12] In addition, these molecules specifically interact with several other RNA receptors, including t-RNA, aptamers, or the viral TAR sequence.[13−16] Finally, they are recognized by the enzymes involved in the drug inactivation that play a central role in bacterial resistance processes.[17] The 3-D structures of several antibiotic/RNA and antibiotic/protein complexes have been described in recent years by X-ray and NMR methods,[7−15,18−20] providing valuable information for the design of new aminoglycoside derivatives.[21]

From a chemical point of view, aminoglycosides are water-soluble oligosaccharides typically functionalized by −three to six ammonium groups. Despite their chemical diversity, most include a modified α-glucose unit (ring I in Scheme 1) attached to position 4 of a 2-deoxystreptamine ring (2-DOS, ring II in Scheme 1). In fact, this disaccharide core constitutes the minimum fragment required for specific binding of the drug to its main biological target, the ribosomal A-site RNA. For the

† Instituto de Química Orgánica General.
‡ Centro de Investigaciones Biológicas.
⊥ Present address: Departamento de Química Universidad de La Rioja.

(1) Greenwood, D. *Antimicbrobial Chemotherapy*; Oxford University Press: Oxford, 1995; pp 32−48.
(2) Walter, F.; Vicens, Q.; Westhof, E. *Curr. Opin. Chem. Biol.* **1999**, *3*, 694−704.
(3) Tor, Y. *ChemBiochem.* **2003**, *4*, 998−1007.
(4) Sucheck, J. S.; Wong, C. H. *Curr. Opin. Chem. Biol.* **2000**, *4*, 678−686.
(5) Hermann, T. *Angew. Chem., Int. Ed.* **2000**, *39*, 1891−1905.
(6) Vicens, Q.; Westhof, E. *ChemBiochem.* **2003**, *4*, 1018−1023.
(7) Vicens, Q.; Westhof, E. *Biopolymers* **2003**, *70*, 42−57.
(8) Fourmy, D.; Recht, M. I.; Blanchard, S. C.; Puglisi, J. D. *Science* **1996**, *274*, 1367−1371.
(9) Carter, A. P.; Clemons, W. M.; Brodersen, D. E.; Morgan-Warren, R. J.; Wimberly, B. T.; Ramakrishnan, V. *Nature* **2000**, *407*, 340−348.
(10) Yoshizawa, S.; Fourmy, D.; Puglisi, J. D. *EMBO J.* **1998**, *17*, 6437−6448.
(11) Vicens, Q.; Westhof, E. *Structure* **2001**, *9*, 647−658.
(12) (a) Vicens, Q.; Westhof, E. *Chem. Biol.* **2002**, *9*, 747−755. (b) Francois, B.; Rusell, R. J. M.; Murray, J. B.; Aboul-ela, F.; Masquida, B.; Vicens, Q.; Westhof, E. *Nucleic Acids Res.* **2005**, *33*, 5677−5690. (c) Kondo, J.; Russell, R. J. M.; Murray, J. B.; Westhof, E. *Biochimie* **2006**, *88*, 1027−1031.
(13) Mikkelsen, N. E.; Johansson, K.; Virtanen, A.; Kirsebom, L. A. *Nat. Struct. Biol.* **2001**, *8*, 510−514.
(14) (a) Jiang, L. C.; Patel, D. J. *Nat. Struct. Biol.* **1998**, 5, 769−774. (b) Jiang, L. C.; Majumdar, A.; Hu, W. D.; Jaishree, T. J.; Xu, W. K.; Patel, D. J. *Structure* **1999**, *7*, 817−827.
(15) Ennifar, E.; Paillart, J. C.; Bodlenner, A.; Walter, P.; Weibel, J. M.; Aubertin, A. M.; Pale, P.; Dumas, P.; Marquet, R. *Nucleic Acids Res.* **2006**, *34*, 2328−2339.
(16) Lapidot, A.; Vijayabaskar, V.; Litovchick, A.; Yu, J.; James, T. L. *FEBS Lett.* **2004**, *577*, 415−421.
(17) Magnet, S.; Blanchard, J. S. *Chem. Rev.* **2005**, *105*, 477−497.
(18) Fong, D. H.; Berghuis, A. M. *EMBO J.* **2002**, *21*, 2323−2331.
(19) Pedersen, L. C.; Benning, M. M.; Holden, H. M. *Biochemistry* **1995**, *34*, 13305−13311.
(20) Vetting, M. W.; Hegde, S. S.; Javid-Majd, F.; Blanchard, J. S.; Roderick, S. L. *Nat. Struct. Biol.* **2002**, *9*, 653−658.
(21) (a) Smith, C. A.; Baker, E. N. *Curr. Drug Targets* **2002**, 2, 143−160. (b) Blount, K. F.; Zhao, F.; Hermann, T; Tor, Y. *J. Am. Chem. Soc.* **2005**, *127*, 9818−9829. (c) Zhao, F.; Zhao, Q.; Blount, K. F.; Han, Q.; Tor, Y.; Hermann, T. *Angew. Chem., Int. Ed.* **2005**, *44*, 5329−5334. (d) Bastida, A.; Hidalgo, A.; Chiara, J. L.; Torrado, M.; Corzana, F.; Cañadillas, J. M.; Groves, P.; Garcia-Junceda, E.; Gonzalez, C.; Jimenez-Barbero, J.; Asensio, J. L. *J. Am. Chem. Soc.* **2006**, *128*, 100−116. (e) Asensio, J. L.; Hidalgo, A.; Bastida, A.; Torrado, M.; Corzana, F.; Junceda, E. G.; Canada, J.; Chiara, J. L.; Jiménez-Barbero, J. *J. Am. Chem. Soc.* **2005**, *127*, 8278−8279.

Scheme 1. Schematic Representation of the α-Glucose/2-DOS Scaffold That, with Different Patterns in the NH_2/NH_3^+/OH Substitution, Is Present in Most Aminoglycosides[a]

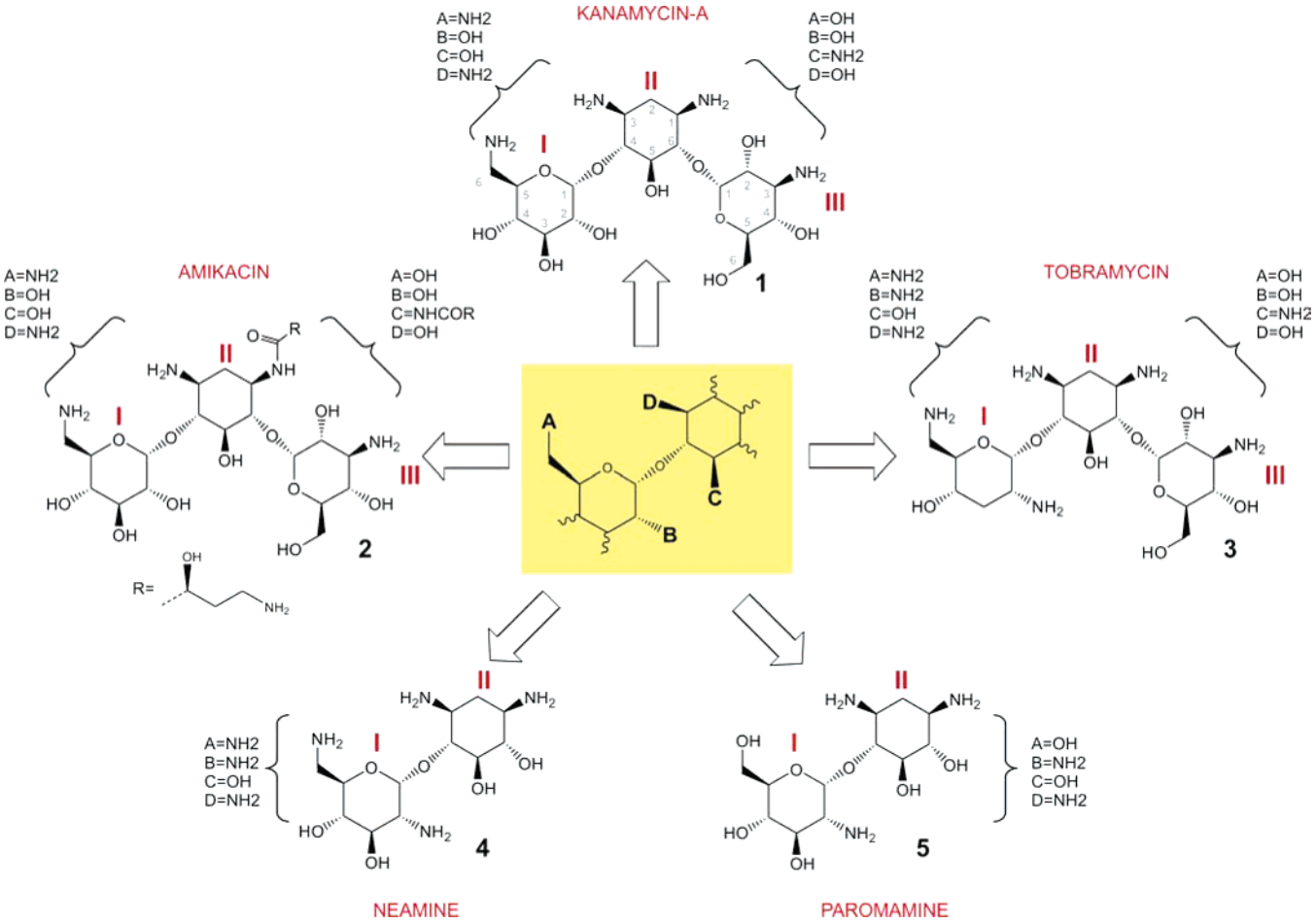

[a] The structures of several antibiotics of the 4,6 2-DOS sub-family and disaccharides including this fragment are shown, as an example. The numbering employed for the different ring positions is represented for **1** (in gray). Finally, the numbering employed for the different sugar units is indicated (in red) in all cases.

so-called 4,6 2-DOS sub-family (see Scheme 1), an additional α-glucose derivative is attached to position 6 of the 2-DOS ring. It should be noted that all aminoglycosides within this sub-family share an identical covalent scaffold and that most interact with the same biological targets. Interestingly, despite these close similarities, they may exhibit a wide range of binding strengths to a given receptor.[22] Certainly, the number and distribution of the amino groups in the aminoglycoside is expected to influence the binding process, as it determines the specific ligand/receptor interactions established in the complexed state. However, it has to be considered that this particular feature might also display a significant effect on the drug conformational preferences or inherent flexibility, which would have obvious consequences on its recognition by proteins or RNA. Interestingly, only a few studies describing the aminoglycoside structural properties, in the free or bound state, have been reported,[23] and little is known about the factors that control their conformation and dynamics. Indeed, this issue is of great interest because it concerns the potential adaptability of these drugs to the spatial and electronic requirements of a given receptor.

Herein, we analyze both theoretically and experimentally the influence that the particular NH_2/NH_3^+/OH distribution present in the antibiotic has on its structure and dynamics and how these features, indeed, affect RNA binding. With this objective, the modified α-glucose/2-DOS fragment (rings I/II or III/II in Scheme 1), present in most aminoglycosides and essential for the interaction of the drug with the ribosomal A-site RNA,[7−12] has been subjected to a careful structural analysis. The obtained results conclusively show that the location of the NH_2/NH_3^+/OH functions, within the covalent structure of the drug, has a significant effect on the conformation and dynamics of these molecules and highlights the conformational controlling role of both charge repulsion and hydrogen-bonding interactions in natural amino sugars. Moreover, according to our data, certain aminoglycoside positions have a key role in the control of the drug structure and flexibility and may, in this way, modulate the strength of the aminoglycoside/RNA interactions without being involved in direct drug/RNA contacts. This work provides simple rules to predict the structure and flexibility of new antibiotic derivatives. Such a predictive capability is a critical component of any drug design strategy.

(22) Wong, C. H.; Hendrix, M.; Priestley, E. S.; Greenberg, W. A. *Chem. Biol.* **1998**, *5*, 397−406.

(23) (a) Asensio, J. L.; Hidalgo, A.; Cuesta, I.; González, C.; Cañada, J.; Vicent, C.; Chiara, J. L.; Cuevas, G.; Jiménez-Barbero, J. *Chem.—Eur. J.* **2002**, *22*, 5228−5240. (b) Asensio, J. L.; Hidalgo, A.; Cuesta, I.; González, C.; Cañada, J.; Vicent, C.; Chiara, J. L.; Cuevas, G.; Jiménez-Barbero, J. *J. Chem. Soc., Chem. Commun.* **2002**, 2232−2233. (c) Hermann, T.; Westhof, E. *Biopolymers* **1998**, *48*, 155−165. (d) Hermann, T.; Westhof, E. *J. Med. Chem.* **1999**, *42*, 1250−1261.

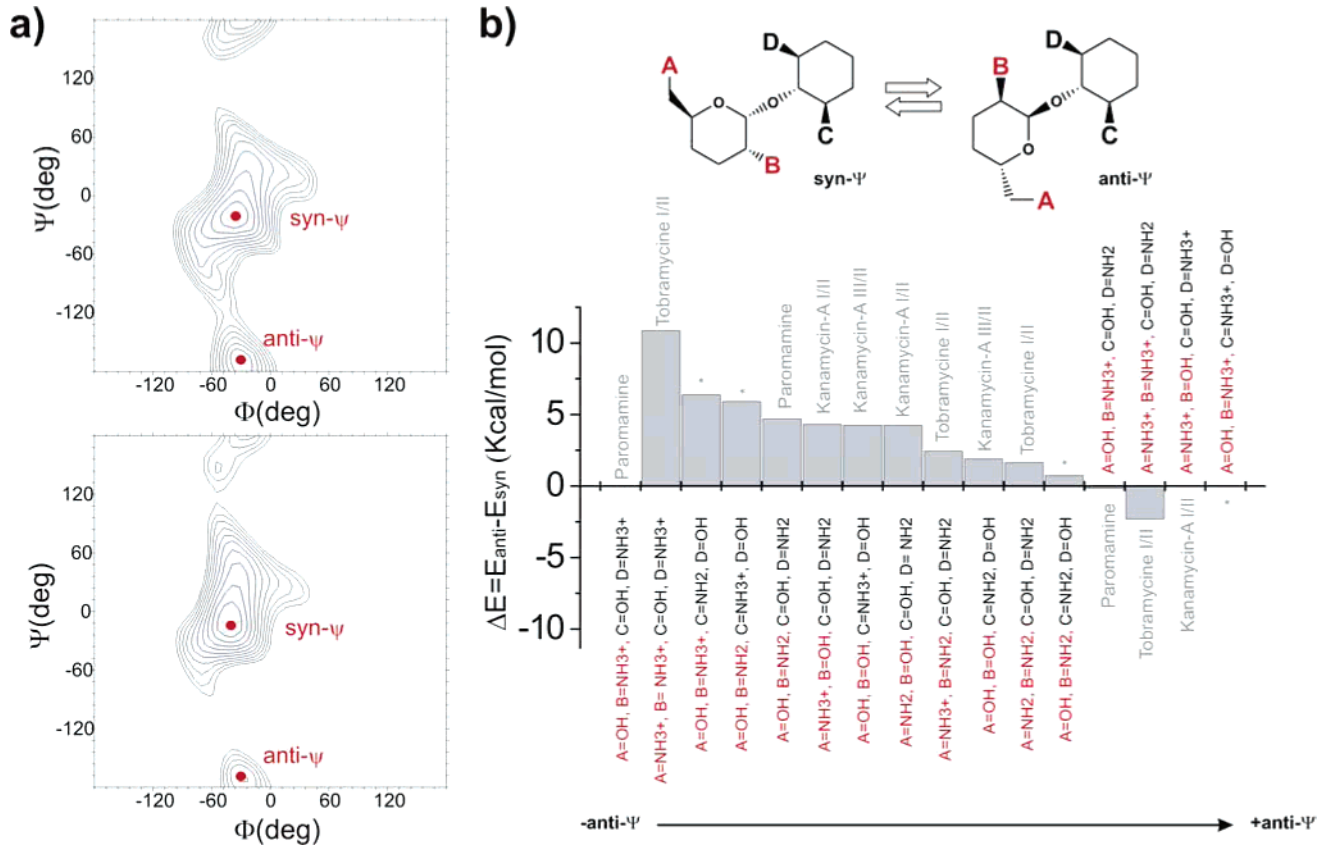

Figure 1. (a) Φ(H1-C1-O1-Cx)/Ψ(C1-O1-Cx-Hx) potential energy surfaces calculated with the AMBER* force field for kanamycin-A I/II (up) and III/II (down) glycosidic linkages. The location of the syn-Ψ/anti-Ψ minima is indicated. (b) Syn-Ψ/anti-Ψ energy differences estimated for the model compound shown in the upper panel, employing DFT calculations. Those distributions not present in natural aminoglycosides are marked with an asterisk. For the A = OH, B = NH_3^+, C = OH, and D = NH_3^+ case, the anti-Ψ geometry is not a minimum. In a similar way, for the A = NH_3^+, B = OH, C = OH, and D = NH_3^+ and A = OH, B = NH_3^+, C = NH_3^+, and D = OH cases, the syn-Ψ geometry is not a minimum.

Results and Discussion

Theoretical Analysis of the Conformational Preferences for the Key Aminoglycoside Fragment α-Glucose/2-DOS. Scheme 1 shows the different α-glucose/2-DOS fragments (rings I/II or III/II) observed in natural aminoglycosides. As a first step in deducing their conformational behavior, the steric maps for two arbitrary NH_2/NH_3^+/OH distributions (those corresponding to kanamycin-A I/II and III/II regions, see Scheme 1) were calculated using the AMBER* forcefield as implemented in MACROMODEL[24] (Figure 1a). These surfaces just provide a first estimation of the conformational regions that are energetically accessible and show the presence of two minima, herein referred to as syn-Ψ (characterized by Ψ values around 0°) and anti-Ψ (with Ψ close to 180°). It seems clear that, to some extent, the energy difference between both geometries will be sensitive to the particular NH_2/NH_3^+/OH distribution present in the aminoglycoside. Moreover, those positions flanking the glycosidic linkage are expected to play a particularly important role in controlling its conformational preferences. To test this hypothesis, DFT optimization of both syn-Ψ and anti-Ψ geometries was performed for the simplified model shown in Figure 1b, considering different combinations of NH_2/NH_3^+/OH groups at these key locations. In all cases, several inter-unit hydrogen-bonding patterns were checked, until the optimal configuration was found. For simplicity, a unique *gg* ($\omega_{N6/O6-C6-C5-O5} = -60°$) orientation was considered for the C_6-N_6/O_6 side chain. Φ/Ψ values of the minima, together with the distances between those groups involved in polar contacts, are shown in the Supporting Information (Table S1).

The obtained results indicate that the preferred orientation around the glycosidic linkage is sensitive to the distribution of polar groups present in the model. In particular, for the A = OH, B = NH_3^+, C = NH_3^+, and D = OH and A = NH_3^+, B = OH, C = OH, and D = NH_3^+ cases, a unique anti-Ψ geometry is predicted (any minimization started from the syn-Ψ structure rapidly converged to the anti-Ψ minimum). This behavior is very unusual in natural *O*-glycosides, for which syn-Ψ populations are typically larger than 95% in solution.[25,26] Interestingly, the A = NH_3^+, B = OH, C = OH, and D = NH_3^+ distribution is present in the protonated form of natural kanamycin-A (compound **1** in Scheme 1). In contrast, for the A = OH, B = NH_3^+, C = OH, and D = NH_3^+ and A = NH_3^+, B = NH_3^+, C = OH, and D = NH_3^+ cases, anti-Ψ geometries are severely destabilized (in fact, for the former, this geometry does not represent a minimum). These two polar group distributions can be found in the protonated forms of natural tobramycin and paromamine (**3** and **5** in Scheme 1), respectively.

(24) Mohamadi, F.; Richards, N. G. J.; Guida, W. C.; Liskamp, R.; Caufield, C.; Chang, G.; Hendrickson, T.; Still, W. C. *J. Comput. Chem.* **1990**, *11*, 440−467.

(25) (a) Asensio, J. L.; Jimenez-Barbero, J. *Biopolymers* **1995**, *35*, 55−78. (b) Asensio, J. L.; Martin-Pastor, M.; Jimenez-Barbero, J. *Int. J. Biol. Macromol.* **1995**, *17*, 137−148.

(26) Dabrowski, J.; Kozar, T.; Grosskurth, H.; Nifantév, N. E. *J. Am. Chem. Soc.* **1995**, *117*, 5534−5539.

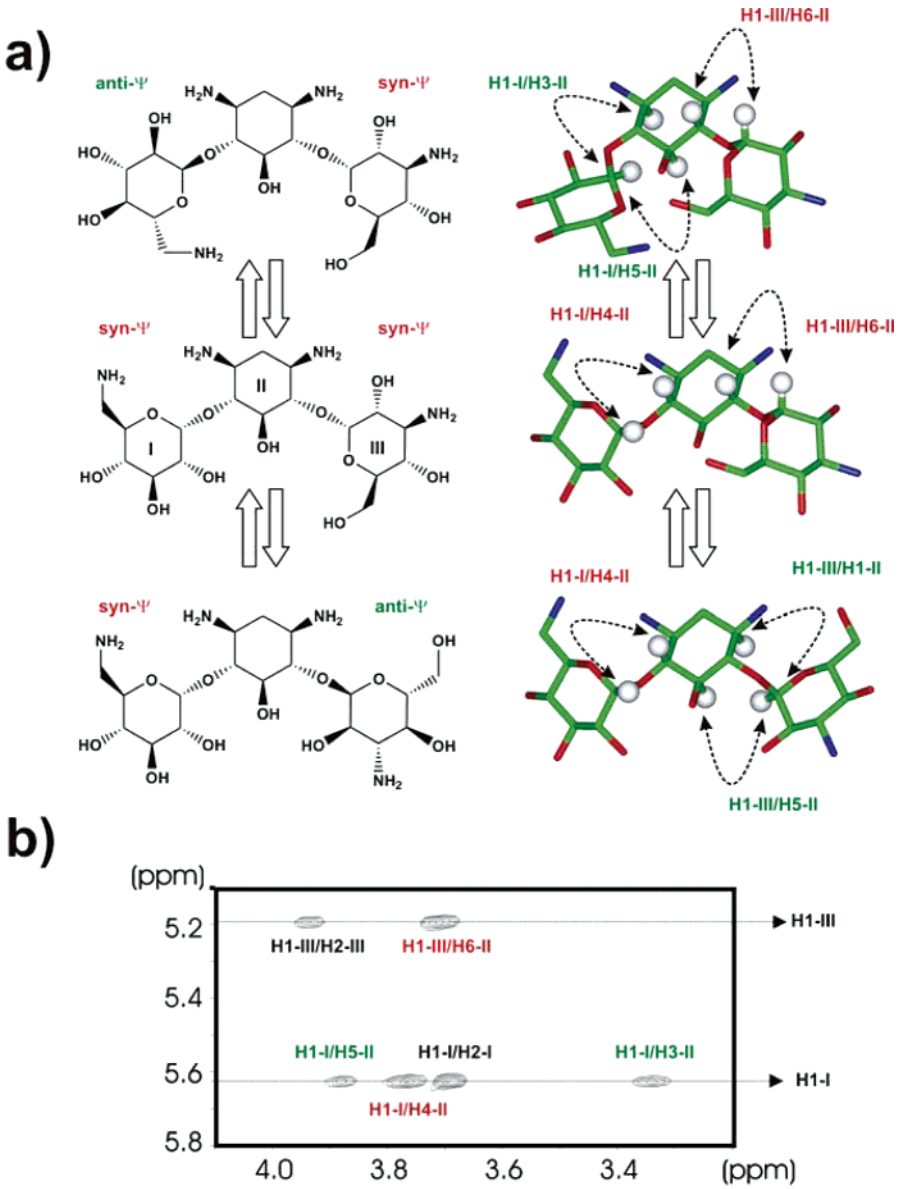

Figure 2. (a) Schematic representation of the minimum energy geometries present for kanamycin-A together with the corresponding exclusive NOEs. (b) Key region of a NOESY spectrum measured for kanamycin-A at 500 MHz, 313 K, and pH 7.0. In all cases, NOEs representative of the syn-Ψ geometry are labeled in red, and those contacts representative of the anti-Ψ minimum are labeled in green.

Taking into account that the bioactive (ribosome-bound) conformation of natural aminoglycosides is, in all cases, syn-Ψ, this peculiar behavior might have a significant effect on the strength of the antibiotic/RNA interaction. However, given the highly charged nature of aminoglycosides and the simplifications assumed in this analysis (no counter ions and a continuous model for the treatment of the solvent), these theoretical predictions should be considered as merely indicative.

Experimental NMR Analysis of the Modified α-Glucose/2-DOS Core. To provide experimental support for the proposed hypothesis, a detailed NMR-based structural study of different natural and synthetic antibiotics and aminoglycoside fragments was performed.

Kanamycin-A (1) Case. Scheme 1 shows the structure of kanamycin-A (**1**) together with the numbering employed for the different sugar units. Interestingly, the DFT calculations, previously described, predict a totally different behavior for the two glycosidic linkages present in this molecule. Thus, for the I/II fragment (A = NH_2/NH_3^+, B = OH, C = OH, and D = NH_2/NH_3^+), an extreme sensitivity of the conformation to the pH conditions is expected, with a major anti-Ψ geometry at acid pH and a major syn-Ψ population at basic pH. In contrast, the syn-Ψ minimum should be dominant for the III/II fragment (A = OH, B = OH, C = NH_2/NH_3^+, and D = OH), under any pH conditions.

The syn-Ψ and anti-Ψ conformations for both linkages, together with the expected exclusive NOEs that unequivocally characterize these geometries, are shown in Figure 2a. Our experimental analysis of the antibiotic conformational properties was carried out at 313 K. First, NMR data for kanamycin-A (**1**) were recorded at pH 7.0. The *J* couplings for the two glucose units and the 2-DOS ring unambiguously show that the $^4C_1$ conformers (with all equatorial substituents) are basically the only detected in solution.

Interestingly, despite the apparent symmetry of the molecule, clear differences between both glycosidic bonds are evident from

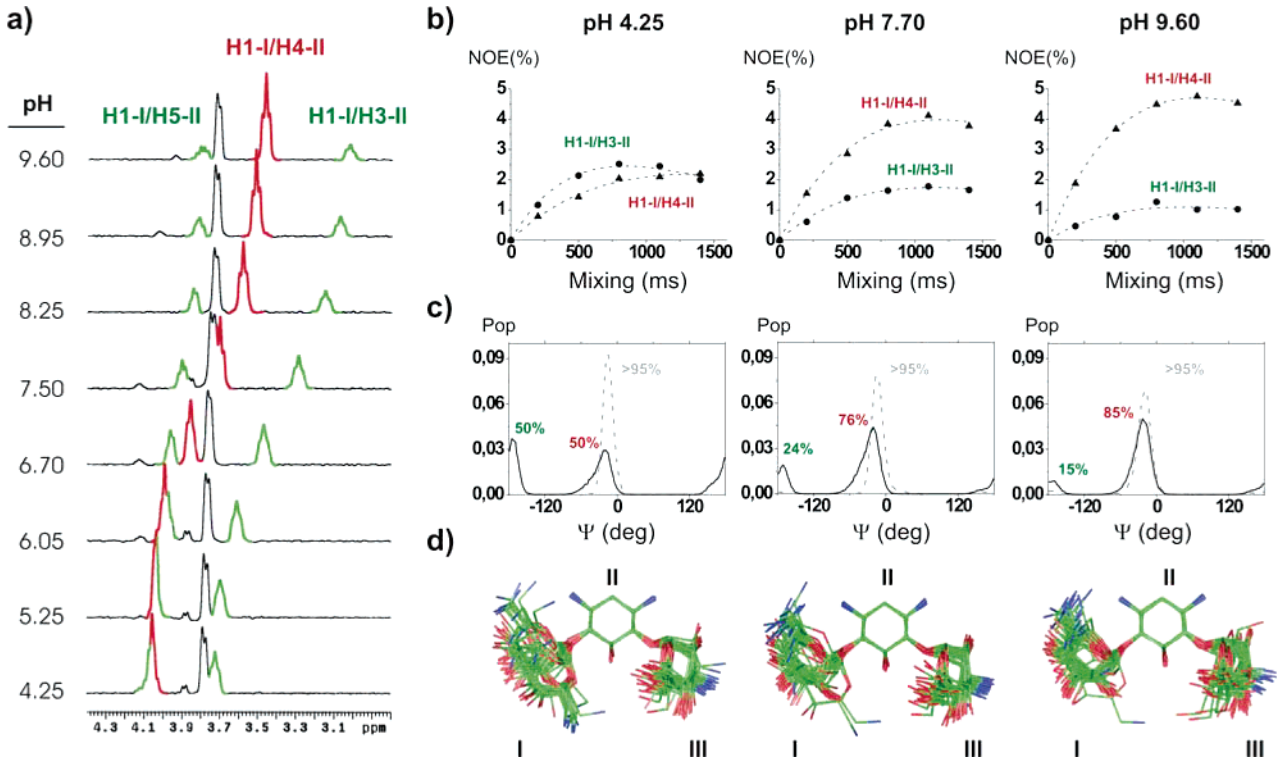

Figure 3. (a) Selective 1-D NOE experiments corresponding to the inversion of H1-I in kanamycin-A, performed at eight different pH values and 313 K. In all cases, NOEs representative of the syn-Ψ geometry are labeled in red, and those contacts representative of the anti-Ψ minimum are labeled in green. (b) Representative NOE build-up curves at three different pH values. The increase in the H1-I/H4-II relative to the H1-I/H3-II cross-relaxation rate, at basic pHs, is evident. (c) MD-tar distributions obtained for the I/II (black) and III/II (dotted gray) ψ angles at these pH values. The different conformational populations are indicated. According to these data, the I/II linkage exhibits a remarkable internal mobility. (d) Ensembles obtained for kanamycin-A, from the previously mentioned experimental data, employing MD-tar simulations.

the inspection of the 2-D NOESY spectra (Figure 2b). Thus, for the I/II linkage (A = NH_2/NH_3^+, B = OH, C = OH, and D = NH_2/NH_3^+), three interresidue contacts (H1-I/H4-II, H1-I/H5-II, and H1-I/H3-II) were observed. These NOEs are not compatible with any single low-energy geometry of the glycosidic linkage and demonstrate the existence of a significant degree of internal mobility for this aminoglycoside region. In fact, the observed NOEs can be easily explained in terms of an equilibrium between syn-Ψ and anti-Ψ minima previously described. The presence in solution of anti-Ψ conformations, for some particular glycosidic linkages, was first suggested by molecular mechanics calculations and later detected by NMR methods.[25,26] Nevertheless, it has to be pointed out that, in all cases, these particular geometries had populations not higher than 5%. In kanamycin-A (**1**), the NOE data are indicative of a remarkably large fraction of anti-Ψ geometries. This conclusion is warranted by the detection of medium-sized H1-I/H5-II and H1-I/H3-II NOE contacts, exclusive of this conformational region. Additional intense NOEs, representative of the anti-Ψ minimum, involving the exchangeable NH_3^+ groups were detected in DMSO, providing strong support for the proposed conformational preference (see Supporting Information Figure S1). A totally different behavior was observed for the III/II glycosidic bond (A = OH, B = OH, C = NH_2/NH_3^+, and D = OH). In this case, a large H1-III/H6-II cross-peak was observed, which is consistent with a major presence of syn-Ψ geometries in solution (see Figure 2b). To assess the pH dependence of the observed behavior, selective 1-D NOE measurements were performed at eight different pH values (Figure 3a). According to the obtained data, the conformation and dynamics of the III/II linkage are rather insensitive to this parameter, with a clear predominance (>95%) of syn-Ψ type geometries in all cases (see Supporting Information). Small H1-III/H5-II and H1-III/H1-II contacts, representative of minor (<5%) anti-Ψ populations, were detectable at neutral and basic pHs, suggesting a rather small increase in the internal mobility under these conditions. In contrast, the structure of the I/II fragment exhibits a clear dependence on the pH (Figure 3a). The NOE-derived distances (some representative values are shown in Table 1) were employed to estimate the conformational distributions at all the pH values tested. With this objective, 80 ns MD-tar[27] (molecular dynamics with time-averaged restraints) simulations were carried out by including the experimental distances as time-average restraints with the AMBER 5.0 program (Figures 3b−d and S2).[28] From the obtained populations, ΔG values corresponding to the syn-Ψ/anti-Ψ equilibrium were determined. The pH dependence of this parameter is represented in Figure 4. It can be observed that, at pH 4.0 (the fully protonated state of the antibiotic), the I/II glycosidic linkage exhibits a remarkable flexibility, with syn-Ψ and anti-Ψ states equally populated. At higher pH values, the fraction of anti-Ψ geometries is gradually decreased from 50% at pH 4.0 ($\Delta G_{\text{syn-}\Psi/\text{anti-}\Psi} = 0$ kcal/mol) to 15% at pH 9.6 ($\Delta G_{\text{syn-}\Psi/\text{anti-}\Psi} = 1.0$ kcal/mol).

To check the accuracy of the estimated conformational populations and as a final control, the conformational distribution of kanamycin-A at different pH values was also determined

(27) Pearlman, D. A. *J. Biomol. NMR* **1994**, *4*, 1−16.
(28) Pearlman, D. A.; Case, D. A.; Caldwell, J. W.; Ross, W. S.; Cheatham, T. E.; DeBolt, S.; Ferguson, D.; Siebel, G.; Kollman, P. *Comput. Phys. Commun.* **1995**, *91*, 1−41.

Table 1. Experimental Distances Obtained from the NMR Analysis of Natural and Synthetic Aminoglycosides **1**−**7** Together with Those Derived from the MD-tar Distributions (in brackets), at Some Representative Values of the pHs Tested[a]

	linkage I/II				linkage III/II			
compound	H1/H4	H1/H3	H1/H5	anti-Ψ (%)	H1/H6	H1/H5	H1/H1	anti-Ψ (%)
1 (pH 4.6)	2.7 (2.7)	2.4 (2.4)	2.4 (2.7)	50	2.3 (2.3)	>3.5 (3.9)	>3.5 (3.7)	<5
1 (pH 9.6)	2.3 (2.5)	2.9 (2.9)	2.7 (3.0)	15	2.2 (2.4)	3.4 (3.4)	3.1 (3.3)	<5
2 (pH 4.4)	2.7 (2.7)	2.4 (2.4)	2.4 (2.7)	53	<2.4	ov	3.2	<5
2 (pH 9.9)	2.3 (2.4)	3.0 (2.9)	2.9 (3.0)	15	<2.4	ov	3.2	<5
3 (pH 3.0)	2.4 (2.3)	>3.5 (4.4)	3.4 (3.6)	<5	2.2 (2.2)	>3.5 (4.4)	>3.5 (3.8)	<5
3 (pH 9.0)	2.4 (2.3)	3.3 (3.4)	3.4 (3.6)	5	2.2 (2.4)	3.3 (3.4)	3.2 (3.4)	5
5 (pH 4.5)	2.3 (2.2)	>3.5 (4.2)	>3.5 (3.9)	<5				
5 (pH 9.0)	2.3 (2.3)	>3.5 (4.3)	>3.5 (3.7)	<5				
6 (pH 4.0)	2.3 (2.5)	2.6 (2.4)	2.6 (2.7)	34	2.3 (2.3)	>3.5 (3.8)	>3.5 (3.7)	<5
6 (pH 7.0)	2.2 (2.5)	2.9 (3.0)	3.0 (3.0)	15	2.2 (2.3)	>3.5 (3.9)	>3.5 (3.7)	<5
7 (pH 4.0)	ov	>3.5	ov	<5	2.3 (2.4)	>3.5 (3.8)	>3.5 (3.6)	<5

[a] For compounds **1**−**5** (shown in Scheme 1), the data correspond to the fully protonated and unprotonated forms of the drugs. Aminoglycoside derivatives **6** and **7** are represented in Figure 9. Anti-Ψ populations estimated in each case are also indicated. ov stands for overlapping NOE. For **7**, distances H1-I/H4-II and H1-I/H5-II could not be determined due to strong overlapping. However, the weak intensity of the H1-I/H3-II cross-peak, corresponding to an average distance larger than 3.5 Å, allows an estimation of the anti-Ψ population.

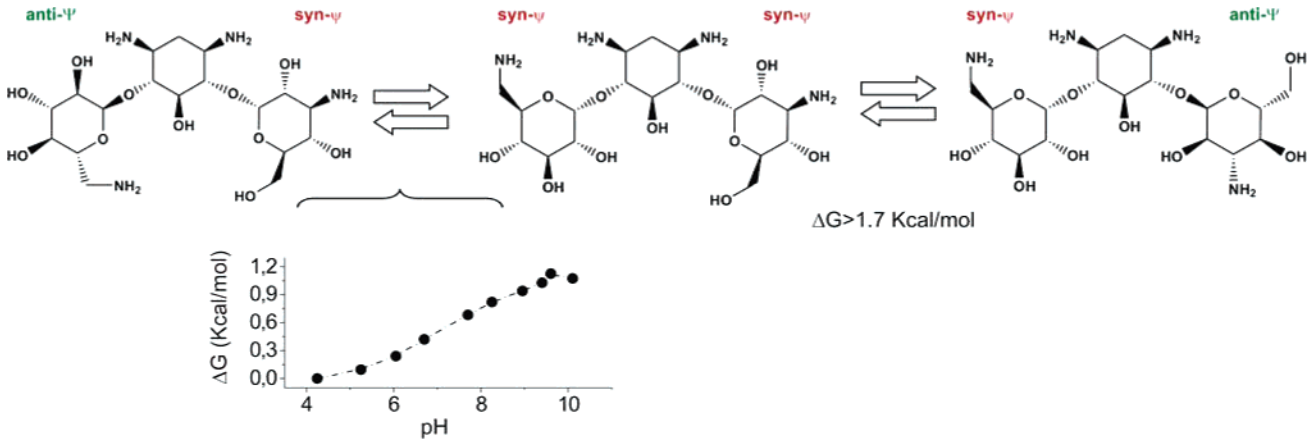

Figure 4. Conformational exchange processes present in kanamycin-A for the I/II (left) and III/II (right) linkages. The free energy differences between the anti-Ψ and the syn-Ψ geometries ($\Delta G = G_{\text{anti}-\Psi} - G_{\text{syn}-\Psi}$), estimated from the NMR analysis, are indicated in both cases.

employing an alternative methodology. Thus, the key NOE build-up curves were fitted with the program CORCEMA (Complete Relaxation and Conformational Exchange Matrix)[29] that allows computation of NOEs (using a full relaxation matrix approach) for systems in chemical exchange. The obtained results (see Figure S3) are in complete agreement with those previously described employing MD-tar calculations (populations obtained employing both methods are within 5% in all cases, see the Supporting Information).

In conclusion, for kanamycin-A (**1**), both glycosidic linkages present rather different conformational properties. The I/II linkage is extremely flexible (especially at acid pH, Figures 3, 4, S2, and S4). In fact, to the best of our knowledge, kanamycin-A (**1**) represents the first case of a natural *O*-glycoside exhibiting up to a 50% population of anti-Ψ structures. In contrast, the III/II linkage behaves like those present in typical α-glycosides, with a fraction of syn-Ψ type geometries >95% in all cases.

Amikacin (2) Case. This antibiotic presents an NH_2/NH_3^+/OH distribution, in the proximities of the I/II linkage (A = NH_2/NH_3^+, B = OH, C = OH, and D = NH_2/NH_3^+), identical to that observed in kanamycin-A (**1**). However, for **2**, the NH_2/NH_3^+ at position 1 of ring II has been replaced by an amide function (see Scheme 1). To show that the unusual structural properties previously described for the I/II fragment in kanamycin-A (**1**) are mainly determined by the particular NH_2/NH_3^+/OH functions flanking the glycosidic bond, and not by long-range interactions with other aminoglycoside regions, the NMR analysis of amikacin (**2**) in solution was also performed. Following the experimental procedure described previously, interproton distances were derived from the analysis of selective 1-D NOE measurements at eight different pH values (Figure 5). The experimental distances were included in MD-tar calculations as restraints to estimate the syn-Ψ/anti-Ψ populations, and the corresponding Δ*G* values were calculated (Figure 5). According to these data, the conformational behavior of **2** is similar to that described for **1**. Thus, the III/II glycosidic bond is fairly rigid, presenting a minor fraction of anti-Ψ conformers (<5%) at all the pH values tested ($\Delta G_{\text{syn-}\Psi/\text{anti-}\Psi}$ > 1.7 kcal/mol). In contrast, the I/II linkage exhibits a remarkable flexibility, which decreases at higher pH values. As shown in Figure 5, the pH dependence of the calculated $\Delta G_{\text{syn}-\Psi/\text{anti}-\Psi}$, for this fragment, closely resembles that observed in kanamycin-A (**1**).

In conclusion, suppression of the positive charge at position 1 of the 2-DOS unit (amikacin vs kanamycin-A) does not affect the structure and flexibility of the I/II antibiotic region. Given the long-range nature of electrostatic interactions, this result could not have been anticipated. Therefore, the unusual conformational properties exhibited by kanamycin-A and amikacin are determined by interactions between units I and II involving

(29) Lee, W.; Rama Krishna, N. *J. Magn. Reson.* **1992**, *98*, 36−48.

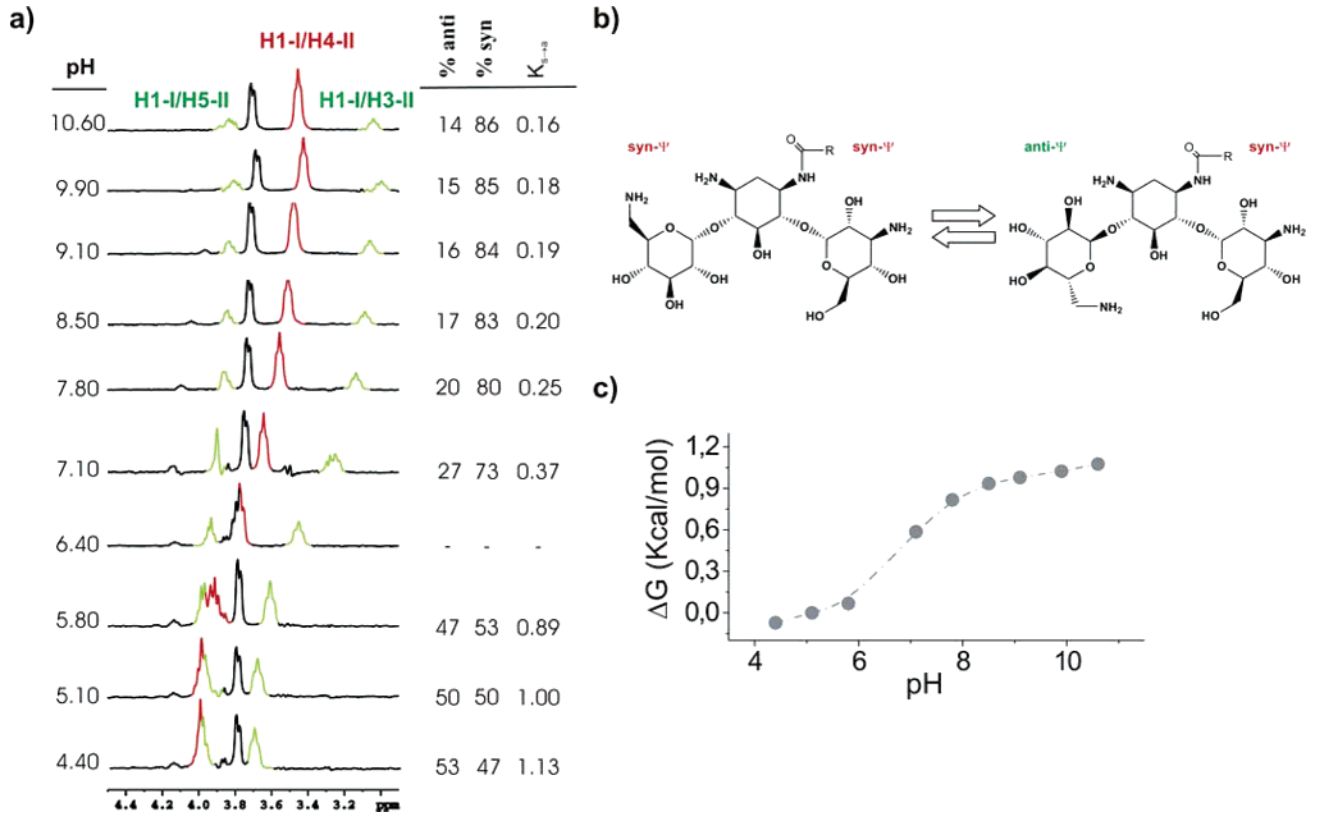

Figure 5. (a) Selective 1-D NOE experiments corresponding to the inversion of H1-I in amikacin performed at eight different pH values and 313 K. In all cases, NOEs representative of the syn-Ψ geometry are labeled in red, and those contacts representative of the anti-Ψ minimum are labeled in green. Syn-Ψ/anti-Ψ populations, estimated from MD-tar calculations, together with the corresponding equilibrium constant are indicated. (b) Conformational exchange process present in amikacin for the I/II linkage. The free energy difference between the anti-Ψ and the syn-Ψ geometries ($\Delta G = G_{\text{anti}-\Psi} - G_{\text{syn}-\Psi}$), as a function of pH, is indicated. The observed behavior closely resembles that previously described for kanamycin-A.

those polar groups flanking the glycosidic linkage (NH_3 6-I, O5-I, OH 2-I, OH 5-II, and NH_3 3-II). This observation highlights the importance of these positions in the conformational control of the drug.

Tobramycin (3) Case. The structure of tobramycin (**3**) is shown in Scheme 1. The III/II fragment is identical to that present in kanamycin-A (**1**) and amikacin (**2**), and therefore, this description of the antibiotic conformational properties will be focused on the I/II linkage. This region (A = NH_2/NH_3^+, B = NH_2/NH_3^+, C = OH, and D = NH_2/NH_3^+) exhibits a NH_2/NH_3^+/OH distribution similar to that present in neamine (**4**) (the disaccharide core common to most aminoglycosides of the neomycin-B family). Figure 6 shows 1-D NOE experiments at two different pH values, together with the corresponding NOE build-up curves. At pH 3.0, a strong H1-I/H4-II contact was detected. The H1-I/H3-II and H1-I/H5-II NOEs, representative of anti-Ψ geometries, were extremely weak (virtually undetectable for the H1-I/H3-II case) at every mixing time tested. This observation proves the exclusive presence of syn-Ψ geometries in solution and is in agreement with the theoretical analysis previously described. At neutral and basic pH values, intense H1-I/H4-II NOEs, indicative of major syn-Ψ populations, were also measured. In addition, minor H1-I/H3-II and H1-I/H5-II contacts were detected, which indicates the existence of a certain fraction of anti-Ψ conformers. However, this population is always below 10%. For example, the NMR data measured at pH 9.0 can be quantitatively reproduced by a 95%/5% syn-ψ/anti-ψ distribution (see Table 1), which is consistent with a free energy difference $\Delta G_{\text{syn}-\Psi/\text{anti}-\Psi}$ around 1.7 kcal/mol (Figure S5). Therefore, the I/II fragment is significantly more rigid in tobramycin than in kanamycin-A. Moreover, the NMR data show that, in contrast with the observed behavior for kanamycin-A, full protonation of tobramycin further decreases its internal mobility (in fact, anti-Ψ populations are below the limit of detection under these conditions).

In conclusion, although kanamycin-A (**1**) and tobramycin (**3**) have similar chemical structures, they exhibit drastically different conformational properties. This observation suggests that position 2 of ring I plays a key role in controlling the geometry and dynamics of the I/II glycosidic linkage. Indeed, the substitution of a single NH_2/NH_3^+ group by an OH causes a dramatic enhancement of the saccharide internal mobility.

Paromamine (5) Case. The structure of paromamine (**5**) (A = OH, B = NH_2/NH_3^+, C = OH, and D = NH_2/NH_3^+) is shown in Scheme 1. This compound has been obtained by methanolysis of the natural antibiotic paromomycin. Figure 7 shows the NOEs measured at different pH values (together with 1-D TOCSY experiments showing the assignment of the key signals from ring II). In all cases, strong H1-I/H4-II interresidue contacts were apparent, demonstrating the almost exclusive presence of syn-Ψ geometries in solution. Very minor H1-I/H3-II NOEs characteristic of the anti-Ψ minimum were only detected at neutral and basic pH values, suggesting a minor increase in the antibiotic flexibility under these conditions. However, even in these cases, the experimental data were consistent with anti-Ψ populations significantly lower than 5%.

General Conclusions from the Structural Analysis of Natural Aminoglycosides. Both theoretical and experimental

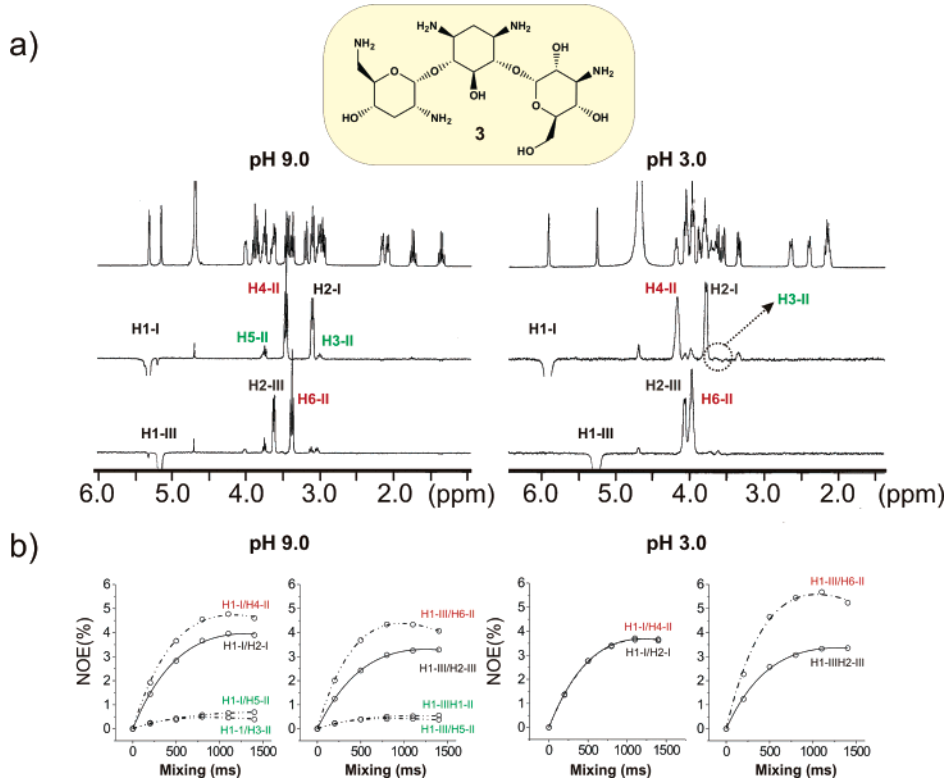

Figure 6. (a) Selective 1-D NOE experiments corresponding to the inversion of H1-I and H1-III in tobramycin, performed at two different pH values and 313 K. In all cases, NOEs representative of the syn-Ψ geometry are labeled in red, and those contacts representative of the anti-Ψ minimum are labeled in green. The absence of the H1-I/H3-II contact at pH 3.0 is highlighted. (b) Representative NOE build-up curves.

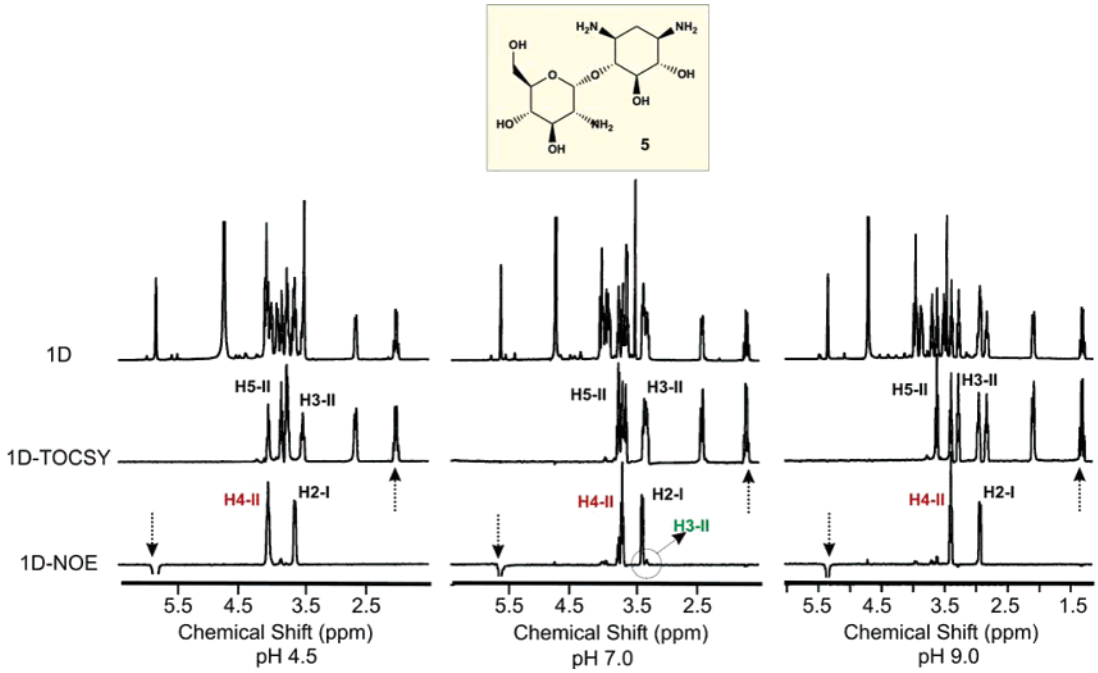

Figure 7. (a) Selective 1-D NOE experiments corresponding to the inversion of H1-I in paromamine, performed at three different pH values and 313 K. An extremely weak H1-I/H3-II NOE is detected at pH 7.0. This contact is clearly absent at acid pH. Selective 1-D TOCSY experiments, showing the assignment of the key signals of the 2-DOS ring, are also shown.

data show that the structure and flexibility of natural aminoglycosides are influenced by the NH_2/NH_3^+/OH distribution present within the antibiotic scaffold. In particular, those positions flanking the glycosidic linkage play a key role in determining the conformational behavior of these molecules. Comparison between those predictions based on the DFT calculations (Figure 1) and the results of the NMR analysis, previously described, indicates that, in general, the theoretical ΔE values for the syn-Ψ/anti-Ψ equilibrium are largely overestimated. This was expected, given the simplifications assumed in this analysis. However, the general trends predicted by the DFT calculations are in agreement with the NMR data. Thus, some particular

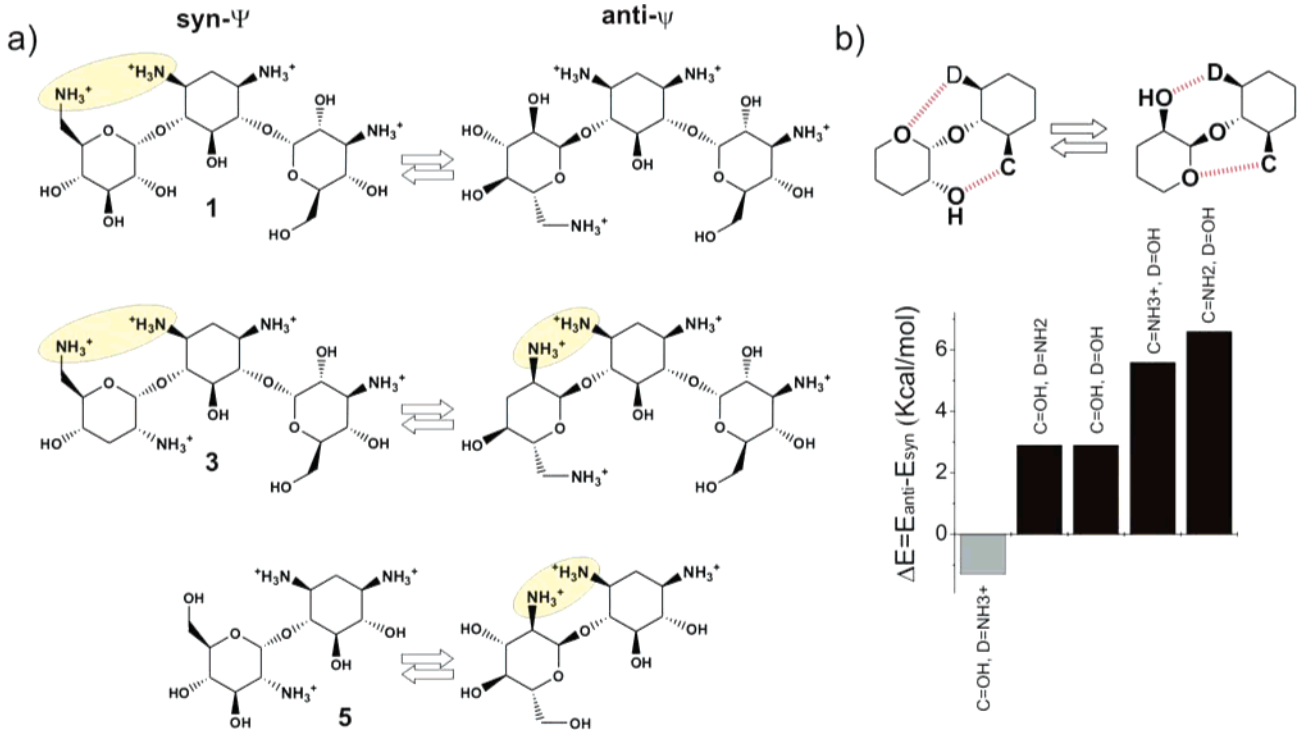

Figure 8. (a) Main charge−charge repulsive interactions present in **1**, **3**, and **5**, between units I and II, for both the syn-Ψ and the anti-Ψ geometries. (b) Syn-Ψ/anti-Ψ energy differences estimated for the model compound shown in the upper panel, employing DFT calculations. The different inter-unit hydrogen-bonding patterns determine its conformational preferences.

NH_2/NH_3^+/OH distributions strongly promote the presence of anti-Ψ geometries in solution. This point has been demonstrated for the I/II linkage in both kanamycin-A and amikacin. Strikingly, a simple OH/NH_3^+ substitution, at position 2 of ring I, causes a drastic change in the conformational preferences of the I/II fragment, locking the glycosidic linkage in a syn-type arrangement (A = NH_3^+, B = OH, C = OH, and D = NH_3^+ vs A = NH_3^+, B = NH_3^+, C = OH, and D = NH_3^+). The DFT calculations predict a unique syn-Ψ geometry for the A = NH_3^+, B = NH_3^+, C = OH, and D = NH_3^+ and A = OH, B = NH_3^+, C = OH, and D = NH_3^+ cases. This point has been experimentally verified for tobramycin I/II fragment and paromamine, under acidic conditions. In these cases, the NOEs representative of the anti-Ψ minimum are extremely weak or below the limit of detection, at any mixing time tested. For the partially protonated forms of the antibiotics, intermediate behaviors between these extreme situations are predicted by the calculations. Our experimental analysis indicates that, in all cases, anti-Ψ geometries are minor (<10%), which prevents their accurate quantification and therefore the estimation of the relative internal mobility of the different aminoglycoside fragments.

Electrostatics versus Hydrogen Bonding as Determinants of Aminoglycoside Conformation. It seems clear that, for polycationic structures like aminoglycosides, the conformational preferences could be strongly influenced by the electrostatic repulsion between the positively charged NH_3^+ groups. This might be sufficient to explain the structural differences observed for the I/II glycosidic bond in kanamycin-A (**1**), tobramycin (**3**), and paromamine (**5**).

Thus, for **1**, the syn-Ψ minimum would be destabilized, at acid pH, by the electrostatic repulsion between positions 6 and 3 of units I and II, respectively (see Figure 8a, upper panel). The distance between these two polar groups is significantly larger in the, usually less stable, anti-Ψ geometry, which might explain the surprisingly large fraction of this conformation detected by NMR. In contrast, for tobramycin (**3**), the presumably stronger, repulsive NH_3^+/NH_3^+ contact, present in the anti-Ψ minimum (Figure 8a, middle panel), would drive the conformational equilibrium toward the syn-Ψ geometry. Finally, for paromamine (**5**), only the anti-Ψ arrangement presents destabilizing NH_3^+/NH_3^+ close contacts, which might explain the rigidity exhibited by this aminoglycoside in the protonated form.

However, in addition to charge/charge interactions, hydrogen bonding must also be taken into account. Indeed, those polar groups flanking the glycosidic linkages might participate in hydrogen bonds, connecting two different units of the antibiotic. Moreover, the different pattern of hydrogen bonds established in the syn-Ψ and anti-Ψ geometries might shift the conformational equilibrium in either direction. To analyze this possibility, a theoretical study was performed, employing the simplified disaccharide model shown in Figure 8b. Thus, the syn-Ψ/anti-Ψ stability difference was evaluated by DFT calculations for different combinations of the polar groups flanking the glycosidic bond. The obtained results are represented schematically in Figure 8b. It can be observed that, in the absence of repulsive contacts between charged groups, hydrogen bonding between the two vicinal units determines the conformational preferences of the model. Interestingly, a major anti-Ψ geometry is predicted, only when the NH_3^+ function is at position D (see Figure 8b). In fact, this particular configuration closely resembles that present in fully protonated kanamycin-A (**1**), which suggests that hydrogen bonding between positions 2 and 3 of units I and II, respectively, might be at the origin of its unusual conformational behavior.

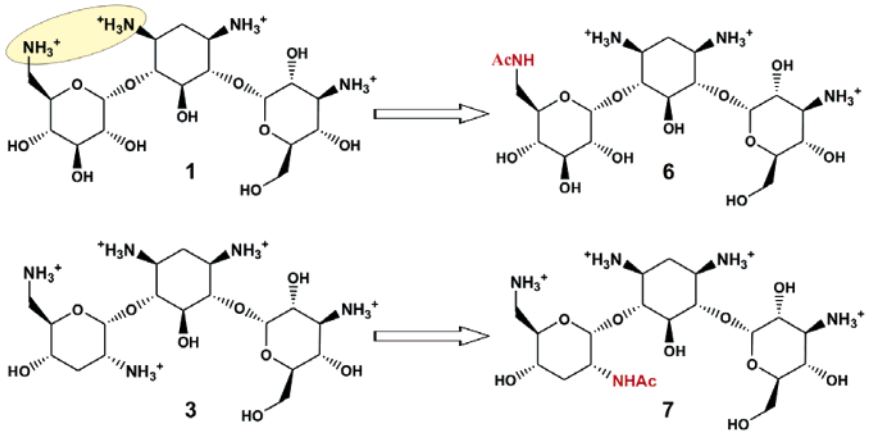

Figure 9. Schematic representation of the synthesized kanamycin-A (**6**) and tobramycin (**7**) monoacyl derivatives. In **6**, the main inter-unit repulsive charge−charge interaction present in the kanamycin-A (**1**) I/II fragment has been removed. Derivative **7** presents a distribution of positive charges, similar to that present in natural kanamycin-A.

To estimate experimentally the relative weight of both charge/charge and hydrogen-bonding interactions, as determinants of aminoglycoside conformation, two simple aminoglycoside derivatives (**6** and **7** in Figure 9) were synthesized and also subjected to a careful NMR analysis. Thus, kanamycin-A (**1**) was selectively acetylated at position 6 of the glucose ring (I) to give **6**, following the procedure described by Hanessian and Patil.[30] In addition, tobramycin (**3**) was acetylated at position 2 of the same sugar unit to give **7**, by employing the enzyme AAC(2′), from *Mycobacterium tuberculosis* (see Figures 9 and S6).[20] In this way, the positive charges present in the natural antibiotics at these two particular positions, over a wide range of pH conditions, were removed. Selective 1-D NOE experiments performed for kanamycin-A and derivatives **6** and **7** are shown in Figure 10.

As previously mentioned, intense H1-I/H3-II and H1-I/H5-II NOEs, indicative of a large anti-Ψ population, are evident for the natural glycoside **1**, at pH 4.0 (Figure 10a). Interestingly, the two contacts are still present, with significant intensity, in **6** (see Figure 10b). In fact, an ca. 34% anti-Ψ population was estimated from the experimental data (see the Materials and Methods, Table 1, and Figure S7). This result is in agreement with the predictions of the theoretical calculations described in Figure 8b. Thus, in the absence of repulsive charge−charge interactions, hydrogen bonding between positions 2 of the glucose ring (I) and 3 of the 2-DOS unit (II) stabilizes the anti-Ψ geometry. At pH 7.1 (Figure 10c), deprotonation of the amino function located at position 3 of ring II shifts the conformational equilibrium toward the syn-Ψ minimum (now 85% population). The weaker hydrogen-bond donor character of the NH_2 versus NH_3^+ functions is at the origin of this behavior. Hydrogen-bonding interactions might also explain the unusual flexibility exhibited by the kanamycin-A/amikacin I/II fragments at neutral pH (with around 30% of anti-Ψ population). Under these conditions, the amino function at position 3 of the 2-DOS ring (ring II) is mainly non-protonated, and thus, this aminoglycoside region is free of charge−charge repulsive interactions. Probably, inter-unit polar contacts established by NH_3^+ located at position 6 of the glucose unit (ring I) stabilize the anti-Ψ arrangement. In fact, close inspection of minimized models indicates that this NH_3^+ group might interact with the OH at position 5 of the 2-DOS ring and even with the OH located at position 6 of the second glucose unit (ring III).

Finally, even in the absence of any positively charged NH_3^+ group flanking the I/II bond (**1** at pH 9.6 or **6** at pH 7.1), this linkage retains an internal mobility (around 15% anti-Ψ population) somewhat larger than that usually observed in typical α-glycosides, which indicates that hydrogen-bonding interactions, involving neutral NH_2/OH functions, can also modulate the saccharide conformational properties.

For the second monoacetyl derivative (**7**, Figure 10d), the NOE data measured at pH 4.0 are indicative of a major syn-Ψ population (>95%). This is in contrast to the behavior exhibited by kanamycin-A (**1**). Therefore, although both **1** and **7** present an identical distribution of positive NH_3^+ groups in the I/II fragment, they exhibit a rather different conformational behavior.

In conclusion, polar groups flanking the glycosidic linkages play a significant role in the conformational control of natural aminoglycosides. Interestingly, although charge−charge repulsive interactions might be dominant for certain NH_2/NH_3^+/OH distributions, the striking conformational properties observed for kanamycin-A (**1**) and amikacin (**2**) mainly result from the presence of inter-unit hydrogen-bonding interactions. In fact, the NOE data measured for kanamycin-A, under high ionic strength conditions (up to 3 M NaCl), reveal a conformational behavior basically identical to that previously described in the absence of salt (see the Supporting Information Figure S8).

Other Conformational Effects: Influence of the Aminoglycoside NH_3^+/OH Substitution Pattern on the Fine Details of the Conformational Distributions. The previous discussion has been focused on the study of the syn-Ψ/anti-Ψ equilibrium in natural and modified aminoglycosides and the way it is influenced by polar contacts between the different antibiotic units. In principle, these interactions might also have a more subtle influence on the precise geometries adopted by a given linkage within both the syn-Ψ or the anti-Ψ low-energy regions. With respect to the anti-Ψ minimum, the potential energy maps previously calculated (Figure 1) show that this geometry is located in a very narrow valley of the surface, and therefore, the distribution of conformers within this area is expected to be rather insensitive to the precise chemical nature of the antibiotic. In contrast, the syn-Ψ geometry (which is dominant for most aminoglycosides) is located on a much wider

(30) Hanessian, S.; Patil, G. *Tetrahedron Lett.* **1978**, *12*, 1035−1038.

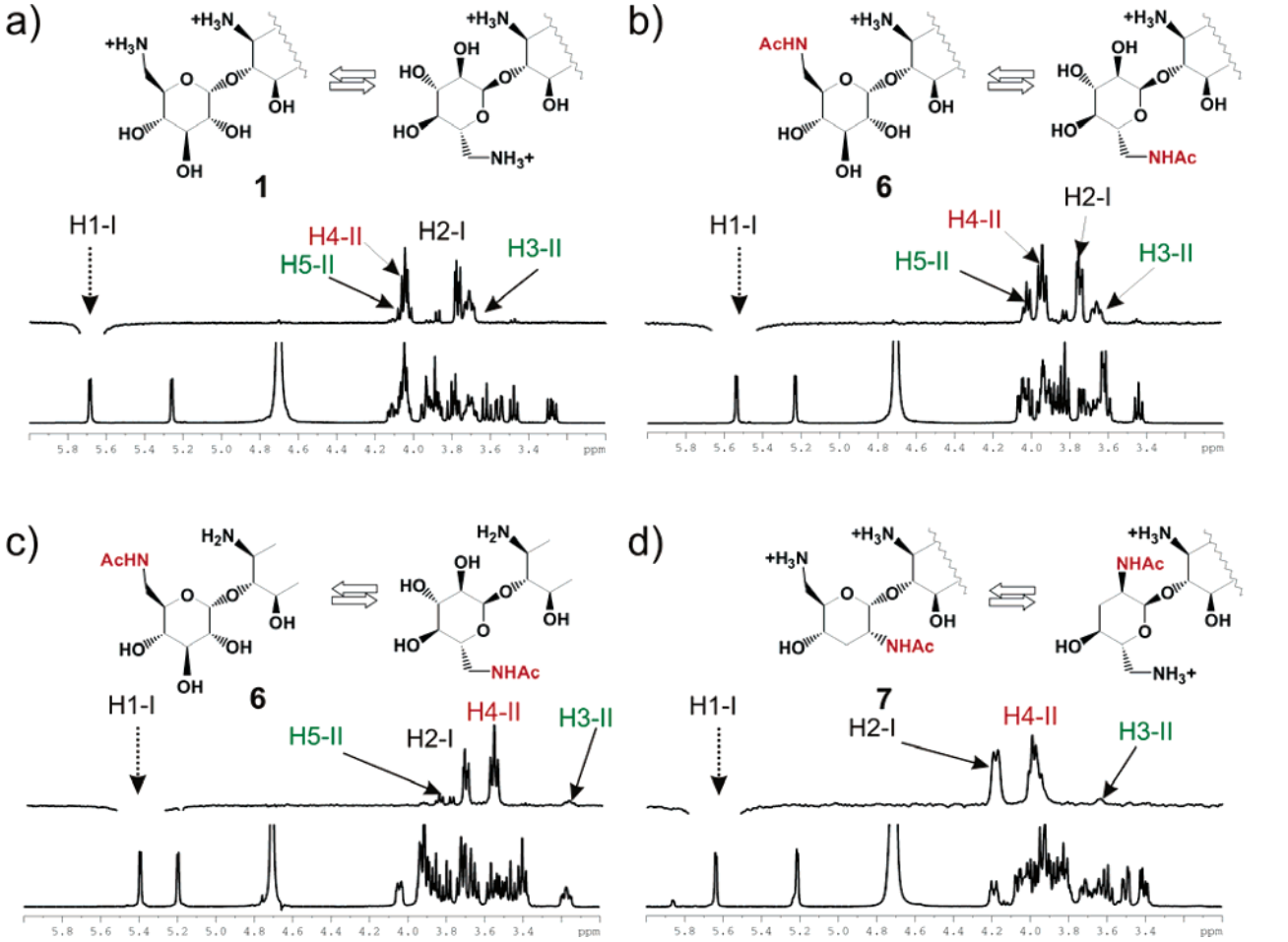

Figure 10. Selective 1-D NOE experiments corresponding to the inversion of H1-I in **1** at pH 4.0 (a), in **6** at pH 4.0 (b), in **6** at pH 7.1 (c), and in **7** at pH 4.0 (d). In all cases, the structurally relevant assignments are indicated.

low-energy valley of the potential energy maps, and hence, the conformational preferences of the drug, within this region, might be slightly affected by its particular NH_2/NH_3^+/OH distribution. In fact, for some aminoglycoside fragments, the existence of deviations in the ϕ angle from those regions favored by the exo-anomeric effect (from $-30°/-70°$ to 0° or even positive values) is even possible. Such unusual conformational behavior has been detected in the past, by our group, for aminoglycosides of the neomycin-B family.[23a,b] Unfortunately, in this case, this assumption cannot be experimentally verified employing NMR since syn-Ψ type geometries are, in all cases, characterized by short H1-I/H4-II or H1-III/H6-II distances, for I/II and III/II fragments, respectively, that is, no NOEs can be used to unequivocally detect and quantify non-exo-anomeric deviations in the glycosidic (Φ) torsion angle. However, a theoretical approach to this problem is certainly feasible.

Figure 11 shows, as contour levels, those ϕ/ψ values characterized by a distance of 3.3 Å (favorable for hydrogen-bonding interactions) between polar pairs at positions O−D, in red, and B−C, in green, for a α-glucose/2-DOS disaccharide, superimposed on the steric map calculated for kanamycin-A I/II fragment. It can be observed that optimal polar contacts between these positions can be simultaneously established at ϕ/ψ values close to $-10°/10°$. In contrast, the sterically favored regions are slightly displaced toward $-40°/-30°$. According to this observation, the distribution of conformers within the central

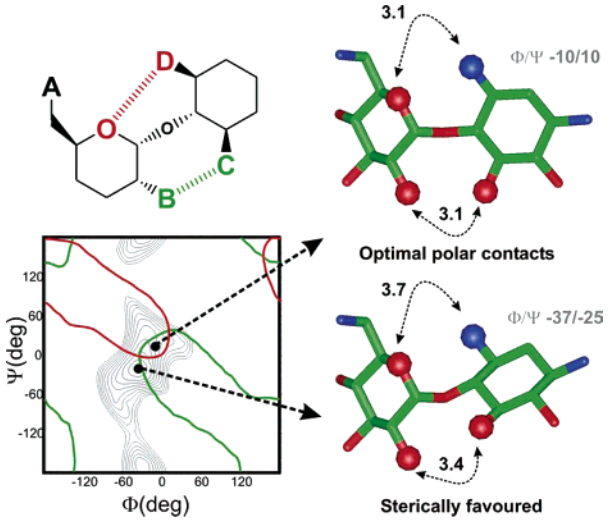

Figure 11. Contour levels showing those ϕ/ψ values characterized by the hydrogen-bonding distance (3.3 Å) between polar atoms O−D (in red) and B−C (in green), superimposed on the steric map calculated for the kanamycin-A I/II fragment. Both polar interactions can be simultaneously established for Φ/Ψ values close to $-10°/10°$. The sterically favored region is centered around $\Phi/\Psi = -40°/-30°$. A geometry representative of both regions is shown on the right.

syn-Ψ low-energy region, exhibited by a particular antibiotic, might be dependent on the relative weight of polar and steric effects.

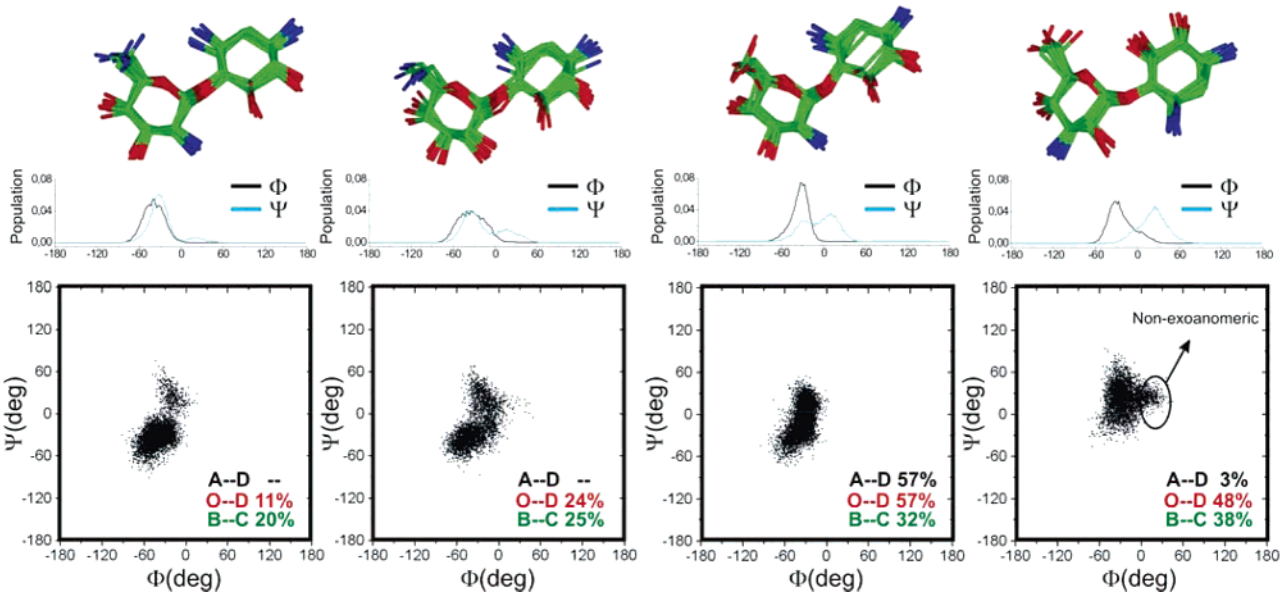

Figure 12. Upper panel: representative ensembles of conformations obtained for the four different disaccharide fragments present in natural aminoglycosides of the 4,6 2-DOS sub-family, from unrestrained solvated 5 ns MD simulations. Middle panel: detailed representation of the distributions obtained for the Φ and Ψ torsion angles (in black and cyan, respectively). Botton panel: conformational distributions, around the low-energy syn-Ψ region, derived from the MD calculations. The fraction of structures along the trajectory, characterized by hydrogen-bonding interactions (d < 3.3 Å) between polar groups pairs A−D, O−D, and B−C (see Figure 11) are shown in black, red, and green, respectively.

The geometrical features, calculated at the PCM/B3LYP/6-31G(d) level, for the syn-Ψ and anti-Ψ minima of the model compounds (represented in Figure 1) are shown in table S1. For the syn-Ψ geometry, most of the minima exhibit low Φ (in the −3°/−25° range) and large Ψ (in the 0°/30° range) values. The observed deviations in Φ toward the eclipsed orientation (Φ = 0°) allow for optimal polar interactions between those groups flanking the glycosidic linkage (the corresponding distances have also been included in table S1).

Considering that, for α-glycosides, Φ is usually in the −30°/−60° range, this observation might suggest a certain tendency to adopt non-exoanomeric conformations (Φ > 0°) for some particular aminoglycoside fragments. However, this preliminary conclusion should be taken cautiously as, given the simplifications assumed in this analysis (no counterions and explicit solvent) and the highly charged natured of aminoglycosides, polar interactions are largely overestimated. Morover, in our opinion, a description of the fine details of the conformational distributions, around the syn-Ψ low-energy region, for the different antibiotic fragments requires explicit consideration of both solvent and counterions. In fact, for neomycin-B, polar interactions between the different sugar units, modulated by subtle solvation effects, were found to be at the origin of its unusual conformational behavior.[23a,b] Interestingly, this could be adequately reproduced by careful solvated unrestrained MD simulations. Taking this into account, we have performed unrestrained MD simulations for different aminoglycoside fragments, employing explicit solvent, counterions, periodic boundary conditions, and Ewald sums for the treatment of electrostatic interactions. Given that polar interactions involving NH_3^+ groups are especially strong, according to the previously described results, this study has been restricted to the fully protonated form of the drugs.

Figure 12 shows the MD trajectories collected for the four different disaccharide fragments found in natural aminoglycosides of the 4,6 2-DOS sub-family. These data strongly suggest that the distribution of conformers around the syn-Ψ region is sensitive to the NH_3^+/OH substitution pattern of the glycoside. Thus, for the neamine core (A = NH_3^+, B = NH_3^+, C = OH, and D = OH), the major population is centered on ϕ/ψ −40°/−30°, which indicates a minor presence of hydrogen bonds between glucose and DOS units. In fact, O5-I and N3-II (position D, see Figure 11) are within hydrogen-bonding distance (<3.3 Å), only 11% of the trajectory. In a similar way, a hydrogen bond involving N2-I/O5-II (positions B and C, respectively, in Figure 11) is present in only 20% of the structures. No hydrogen-bonding contacts were detected between positions A and D. A different behavior was observed for the III/II fragment present in kanamycin-A and tobramycin (A = OH, B = OH, C = NH_3^+, and D = OH). In this case, the conformational distribution is slightly displaced toward larger ψ values (in fact, ψ is positive for most of the structures). Moreover, the ϕ angle distribution is clearly extended toward larger values, adopting, for a minor fraction of structures, orientations not favored by the exo-anomeric effect (ϕ > 0). Significant deviations from the exo-anomeric regions have been detected, by our group, for the ribose unit present in aminoglycosides of the neomycin-B family.[23a,b] The obtained data suggest that the III/II fragment present in kanamycin-A and tobramycin might exhibit a slight tendency to adopt non-exoanomeric orientations. This conformational behavior has its origin in the presence of polar interactions between both units of the disaccharide. Thus, the O5-III/O5-II (interaction O−D in Figure 11) and O2-III/N1-II (positions B and C in Figure 11) hydrogen bonds are present in 48 and 38% of the structures along the MD trajectory, respectively.

As previously mentioned, the conformational behavior predicted for neamine and fragment III/II of kanamycin-A by the simulations cannot be unambiguously distinguished by NMR since, in both cases, the only strong interresidue NOE expected is that involving those protons flanking the glycosidic linkage (H1-I/H4-II for neamine and H1-III/H6-II for disaccharide III/

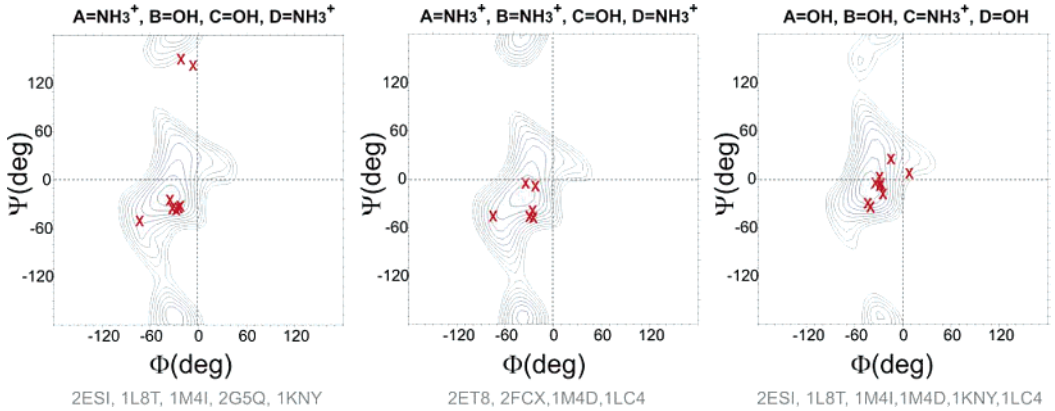

Figure 13. Φ/Ψ values observed for some aminoglycosides of the 4,6 2-DOS sub-family and disaccharides (neamine) in complex with both RNA and protein receptors, according to X-ray studies, superimposed on the steric maps calculated for the different glycosidic linkages. The nature of those polar groups flanking the glycosidic linkages (A−D) is indicated above. The PDB codes of the complexes are shown at the bottom of the figure.[12,13,18−20]

II). However, there are slight differences in the average interproton distances derived from the MD trajectories. Thus, for neamine, the average H1-I/H4-II distance ($<r^{-6}>^{-1/6}$) is 2.4 Å, and therefore, a NOE similar to the reference intraresidue H1-I/H2-I cross-peak would be expected. In contrast, for fragment III/II of kanamycin-A or tobramycin, the average H1-III/H6-II distance is shorter (2.2 Å), and therefore, the corresponding NOE should be significantly more intense than the reference intraresidue H1-III/H2-III contact. This prediction is in agreement with the NMR measurements previously described. Indeed, for the fully protonated form of tobramycin, the I/II fragment exhibits a $\sigma_{H1-I/H4-II}/\sigma_{H1-I/H2-I}$ ratio equal to 1.0. In contrast, the ratio $\sigma_{H1-III/H6-II}/\sigma_{H1-III/H2-III}$ measured for the III/II fragment is 1.9 (see Figure 6b). This observation is in agreement with the MD trajectories collected and suggests a slightly different distribution of conformers, within the syn-Ψ region, for both glycosidic linkages.

For the kanamycin-A I/II (A = NH_3^+, B = OH, C = OH, and D = NH_3^+) linkage and paromamine (A = OH, B = NH_3^+, C = OH, and D = NH_3^+), intermediate situations between those previously described were found, with conformational distributions progressively more extended toward positive ψ regions.

In conclusion, our theoretical analysis strongly suggests that the fine details of the conformational distribution, within the syn-Ψ low-energy region, present for a given α-glucose/2-DOS fragment are also affected by its pattern of NH_3^+/OH substitution. Polar contacts between the two units, modulated by the differential solvation of the groups involved, seem to be at the origin of this effect.

Receptor Bound Conformation of Aminoglycosides. The structures of several aminoglycosides between those represented in Scheme 1, complexed to different protein and RNA receptors, have been described in recent years employing X-ray crystallography. Herein, we have shown that their conformational preferences, in the free state, are modulated by the distribution of NH_2/NH_3^+/OH groups present within the aminoglycoside scaffold. Obviously, in the complexed state, the geometries adopted by these molecules will also be strongly determined by the topological features of the receptor binding pocket. In fact, according to several studies, both aminoglycosides and RNA binding regions are capable of a high degree of conformational adaptation.[23,31] However, it should be kept in mind that any deviation from the inherent conformational preferences of the glycoside would represent an energy penalty that should be compensated by additional stabilizing ligand/receptor interactions to maintain the binding strength. Therefore, a previous knowledge of these conformational preferences might help to understand the energy balance of the binding process.

Figure 13 shows the conformation adopted by the I/II and III/II linkages, present in several aminoglycosides of the 4,6 2-DOS sub-family and disaccharide fragments (neamine), in complex with different protein and RNA receptors, according to X-ray data, superimposed on the corresponding steric surfaces. Although a significant dispersion in the ϕ/ψ values is observed in all cases, reflecting the diverse features of the binding sites and the large adaptability of these ligands, these data are also in qualitative agreement with the conformational preferences previously described for each linkage. Thus, for the kanamycin-A and amikacin I/II fragments (A = NH_3^+, B = OH, C = OH, and D = NH_3^+), most of the structures are clustered around the central syn-Ψ low-energy region. However, anti-Ψ geometries are also found in the complexed state. In fact, this orientation has not been detected, in the bound state, for any other aminoglycoside within this sub-family. This observation is in agreement with the large flexibility exhibited by kanamycin-A in solution. In fact, according to the NMR data, the syn-Ψ/anti-Ψ transition represents, for the protonated form of the drug, a ΔG cost close to 0. For the tobramycin I/II region and neamine (A = NH_3^+, B = NH_3^+, C = OH, and D = NH_3^+), the distribution is scattered around the syn-Ψ minimum, and a similar behavior is exhibited by the kanamycin-A/tobramycin III/II fragments (A = OH, B = OH, C = NH_3^+, and D = OH). However, in the latter case, the distribution seems to be slightly shifted toward larger ϕ/ψ values. Moreover, a non-exo-anomeric orientation of the glycosidic torsion angle ($\phi > 0$) is detected in one of the aminoglycoside/receptor complexes. In fact, the experimental distribution observed for this linkage closely resembles that previously deduced for the free state, employing MD simulations (see Figure 12). In conclusion, all these observations are in agreement with the conformational prefer-

(31) (a) Tor, Y.; Hermann, T.; Westhof, E. *Chem. Biol.* **1998**, *5*, 277−283. (b) Shandrick, S.; Zhao, Q.; Han, Q.; Ayida, B. K.; Takahashi, M.; Winters, G. C.; Simonsen, K. B.; Vourloumis, D.; Hermann, T. *Angew. Chem., Int. Ed.* **2004**, *43*, 3177−3182. (c) Hermann, T.; Westhof, E. *J. Mol. Biol.* **1998**, *276*, 903−912.

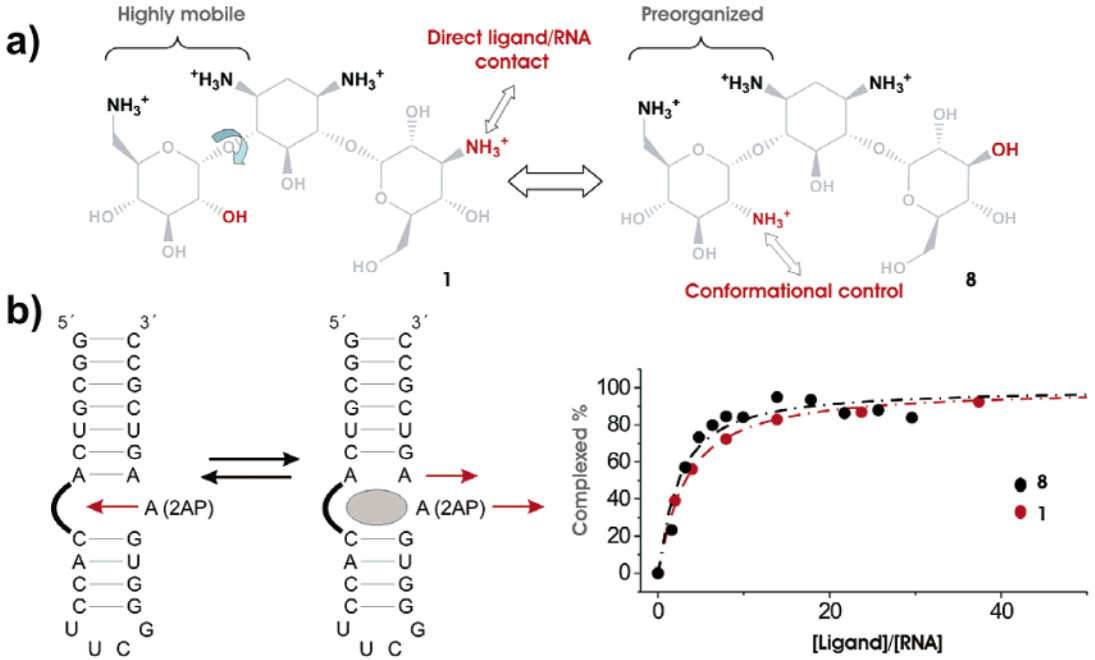

Figure 14. (a) Schematic representation of kanamycin-A (**1**) and derivative **8**. Both compounds differ exclusively in the location of a single amino group. (b) Left: schematic representation of the modified RNA fragment employed in our binding studies and the structural change induced by aminoglycoside binding. Right: some representative binding curves obtained for kanamycin-A (**1**, red) and derivative **8** (black) under identical conditions.

ences previously described (both theoretically and experimentally) for the free state and suggest that aminoglycoside receptors tend to recognize geometries within the main low-energy region of the ligand, which, according to our results, can be different even for two antibiotics of the same family, depending on their particular pattern of NH_2/NH_3^+/OH substitution.

Aminoglycoside Flexibility and RNA Binding. It is well-established that the number and particular distribution of positive charges within the aminoglycoside scaffold play a key role in its molecular recognition by RNA.[31c,32] Thus, ammonium groups may compete with Mg^{2+} for binding sites located on the RNA ternary fold, as proposed for the hammerhead ribozyme.[31c] Moreover, they participate in a number of specific polar interactions involving both phosphates and neutral groups.[7−12] Herein, we have shown that the NH_2/NH_3^+ groups play an additional role in modulating the antibiotic conformation or inherent flexibility. This fact might have an influence on the aminoglycoside/RNA recognition properties, especially in those cases in which the antibiotic internal mobility is severely restricted upon binding or when conformations different from the global minimum are selected by the receptor. To find experimental support for this hypothesis, the aminoglycoside derivative **8** (shown in Figure 14a) was synthesized, and its affinity for the A-site RNA was compared to that exhibited by natural kanamycin-A (**1**, see Figure 14). Both **1** and **8** present the same number of amino groups (the total charge of the antibiotic is not altered) and exclusively differ in the location of a single NH_2/NH_3^+ function; the amino group located at position 3 of ring III (in **1**) has been moved to position 2 of ring I (in **8**). This modification is expected to display two opposite effects on the binding affinity of **8** to RNA. First, it has to be considered that the amino group at unit III (in **1** and **3**) is involved in a direct hydrogen bond with G1405 within the antibiotic/A-site complex.[12] This interaction is known to be important for both aminoglycoside affinity and specificity.[33,34] In fact, a 16−50-fold decrease in biological activity has been reported for a kanamycin-B derivative bearing an OH group at this particular position.[34] In contrast, the NH_2/NH_3^+ present at position 2 of ring I (for **3**, **4**, or also for derivative **8**) is not involved in any direct aminoglycoside/RNA contact according to X-ray data.[12] Thus, taking this fact into account, **8** should present a significantly lower affinity for the A-site RNA than that exhibited by kanamycin-A (**1**). However, as a second point, we have shown previously that this particular function locks the key I/II fragment in the bioactive (according to X-ray data) syn-Ψ orientation. This fact was also experimentally verified for **8** by using NMR (see Figure S9). Therefore, this antibiotic region is already preorganized for RNA binding. In contrast, for **1**, the I/II linkage is characterized by a significant fraction of the anti-Ψ population (around 50% in the fully protonated form) and an unusually large internal mobility. According to this second point, a larger entropic barrier (and lower affinity) would be expected for the molecular recognition of **1** by the RNA receptor.

The relative importance of both enthalpy- and entropy-favored issues was deduced by performing binding studies, employing the fluorescence-based approach developed independently by Pilch[35] and Hermann.[36] This methodology makes use of a modified 27-mer RNA fragment (A-site-(2AP)), which includes the A-site sequence, with the fluorescent base analogue 2-aminopurine (2AP) replacing A1492 (Figure 14b). It is well-established that, for this system, aminoglycoside binding causes a marked increase in the fluorescence intensity at 369 nm. Thus,

(32) Wang, H.; Tor, Y. *J. Am. Chem. Soc.* **1997**, *119*, 8734−8735.
(33) Wang, J.; Li, J.; Cheng, H.; Chang, H.; Tanifum, C. T.; Liu, H.; Czyryca, P. G.; Chang, C. T. *J. Med. Chem.* **2004**, *6*, 1381−1384.
(34) Li, J.; Wang, J.; Czyryca, P. G.; Chang, H.; Orsak, T. W.; Evanson, R.; Chang, C. T. *Org. Lett.* **2004**, *6*, 1381−1384.
(35) Kaul, M.; Barbieri, C. M.; Pilch, D. S. *J. Am. Chem. Soc.* **2004**, *126*, 3447−3453.
(36) Shandrick, S.; Zhao, Q.; Han, Q.; Ayida, B. K.; Takahashi, M.; Winters, G. C.; Simonsen, K. B.; Vourloumis, D.; Hermann, T. *Angew. Chem., Int. Ed.* **2004**, *43*, 3177−3182.

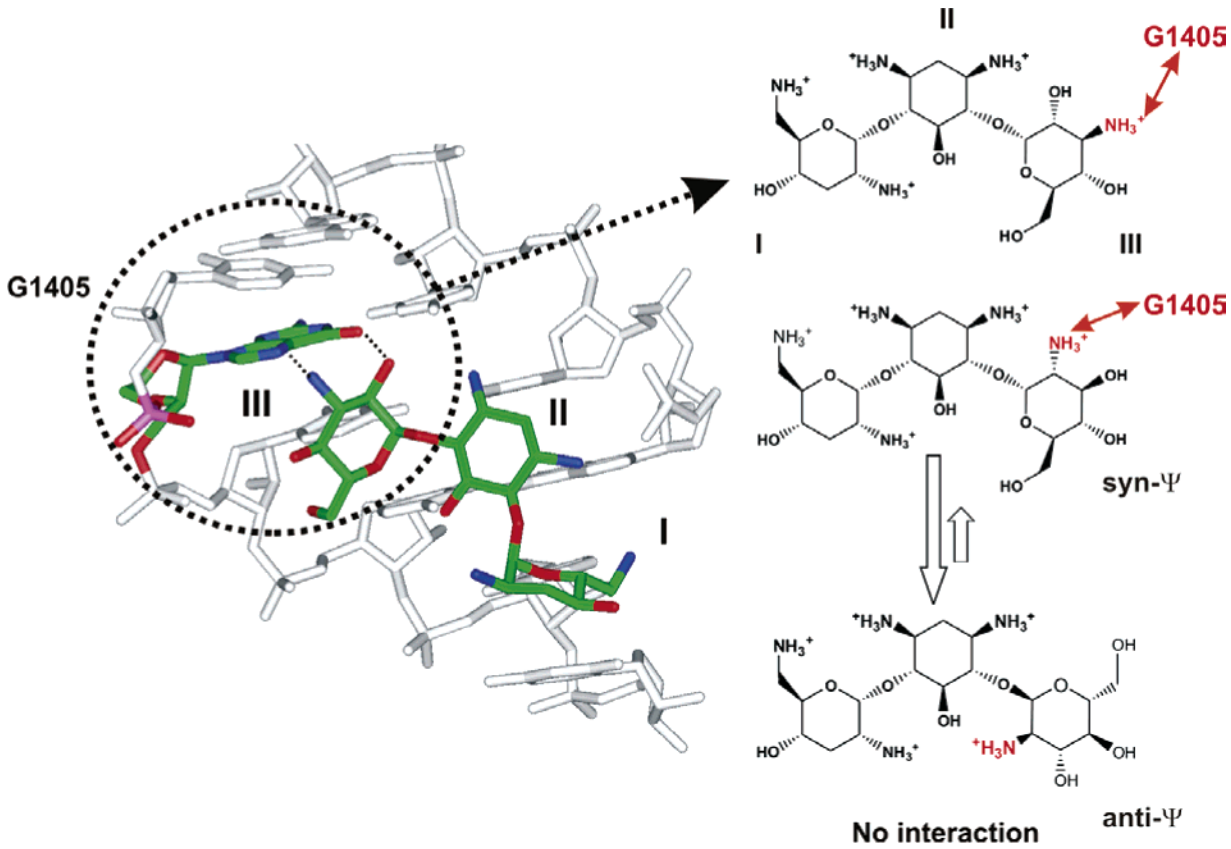

Figure 15. Left: structure of the tobramycin/A-site complex according to X-ray data.[12] Interactions between positions 2 and 3 of ring III with G1405 are highlighted. Right: according to our theoretical and experimental analysis, a NH_3^+ group located at position 2 of this unit would shift the conformational equilibrium toward the not bioactive anti-Ψ arrangement.

the observed changes were monitored as a function of the [drug]/[RNA] ratio in titration experiments, and K_d values were derived.

Typical binding curves are shown in Figure 11b. The K_d values measured for kanamycin-A (**1**) and derivative **8** were of 5.5 and 3.8 μM, respectively, reflecting similar binding affinities for both the natural and the synthetic aminoglycosides. Given that the amino function present at position 3 of ring III is known to play a significant role in the A-site recognition,[34] this result strongly suggests the existence of a compensating contribution for derivative **8**. In our opinion, the higher degree of preorganization exhibited by this aminoglycoside is the most likely explanation for the observed behavior. Thus, although it is not involved in direct interaction with the RNA receptor, the amino function at position 2 of ring I contributes to binding, by locking the key I/II antibiotic region in its bioactive conformation. The relevance of this particular position in the conformational control of the drug might explain why it is occupied by an NH_2/NH_3^+ function in most aminoglycosides (despite the fact that it does not participate in direct ligand/receptor contacts).

Attempts have been made in the past to exploit the decrease in conformational entropy of aminoglycosides by either locking or biasing conformations toward the bioactive one.[21] Strikingly, according to the reported results, this does not seem to be a particularly effective strategy for the design of new aminoglycoside antibiotics with a larger affinity for the RNA receptors, which might suggest a minor contribution of the ligand conformational entropy to the global ΔG. However, it should be mentioned that, in all cases, the conformational restriction of the aminoglycoside was achieved by means of a covalent modification that implied the removal of key polar groups of the drug, presumably required for tight binding. In addition, according to X-ray data,[21c] the constrained derivatives presented a different orientation of one of the sugar units, within the RNA binding pocket, establishing a different pattern of interactions with the receptor. In our opinion, an enthalpy−entropy compensation phenomenon is probably cancelling out any potential benefit derived from the decrease in the ligand conformational entropy, rendering the approach less useful than expected.

The relationship between the NH_2/NH_3^+/OH distribution and aminoglycoside conformation has not been appreciated in the past and might help to rationalize some observations recently described in the literature.[34] For example, according to X-ray data,[12] the OH group located at the position 2 of ring III also donates a hydrogen bond to G1405 within the tobramycin/A-site complex (Figure 15). In fact, this location seems adequate for a NH_3^+ group, if we exclusively aim to optimize the ligand/receptor interactions. According to this hypothesis, the displacement of the amino function from position 3 to 2 should have a minor effect on the complex stability or even produce a further stabilization. A kanamycin-B derivative including this modification has been recently synthesized by Chang et al.[34] as a part of a library of aminoglycoside analogues. The measured MIC values suggest a significant decrease in activity of this molecule (8−16-fold decrease) with respect to that exhibited by the natural compound. Our data provide a simple explanation for this behavior. Thus, this particular distribution of polar groups (A = OH/B = NH_3^+/C = NH_3^+/D = OH, see Figure 1b) produces a significant alteration of the conformational preferences of the III/II fragment, driving the equilibrium far from the bioactive arrangement toward the anti-Ψ geometry (Figure 15). In fact,

this is the only minimum found by the DFT calculations, as described previously (Figure 1b). Obviously, the syn-Ψ geometry might still bind to the RNA receptor, but, in any case, the recognition of a high energy conformation implies a certain ΔG penalty that, in this case, does not seem to be compensated by additional ligand/receptor contacts. Not surprisingly, this particular distribution of amino groups is not found in any natural antibiotic. According to the results reported by Chang et al.,[34] position 3 of unit III represents the optimal location for a NH_2/NH_3^+ group. Certainly, this position allows for optimal drug/RNA contacts without inducing significant alterations in the structure of the aminoglycoside. In conclusion, our results strongly suggest that the influence of the NH_3^+/NH_2/OH distribution on the structure of aminoglycosides should be taken into account in the design of new drug derivatives.

Conclusion

We have proved both theoretically and experimentally that the particular distribution of amino functions, within the aminoglycoside scaffold, has a significant influence on the conformational preferences and inherent flexibility of these antibiotics. Indeed, for the modified α-glucose/2-DOS core (I/II or III/II fragments), present in most aminoglycosides, a range of internal mobilities is detected, depending on the location of the NH_2/NH_3^+/OH functions.

Our results highlight the key role of the polar groups flanking the glycosidic linkages for the conformational control of these drugs. In fact, a single OH/NH_3^+ replacement at these key positions can have a dramatic effect on the antibiotic conformation in solution (i.e., kanamycin-A vs tobramycin conformation). The NMR analysis of simple aminoglycoside derivatives demonstrates that, although charge−charge repulsive interactions might be dominant for certain NH_2/NH_3^+/OH distributions, hydrogen bonding also plays a significant role in modulating the conformational preferences of these molecules.

Finally, our data suggest that the NH_2/NH_3^+/OH distribution could indirectly modulate the antibiotic RNA binding properties, by affecting their conformational preferences. This fact should be taken into account for the design of new aminoglycoside-based antibiotics. Thus, those particular patterns of substitution that promote a significant destabilization of the antibiotic bioactive conformation are expected to have, for this reason, an unfavorable contribution to the energy balance of the binding process that might be, or not, compensated for by other factors. In contrast, for those substitutions that stabilize the bioactive conformation, this unfavorable contribution will be absent. Intriguingly, position 2 of ring III is not occupied by an amino function in any natural aminoglycoside of the 4,6 2-DOS subfamily, despite the fact that, according to the structural data available, it might establish optimal interactions with the A-site RNA. In contrast, position 2 of ring I is, in most cases, occupied by an amino group, although it does not participate in any direct aminoglycoside/RNA contact. Both observations suggest that, in fact, the NH_2/NH_3^+/OH distribution present in natural antibiotics might have been optimized by evolution to fine tune not only the receptor/ligand contacts but also the aminoglycoside conformational properties. These features, which are of general interest for conformational studies of (bio-)organic molecules, are also relevant for molecular recognition and drug design.

Materials and Methods

Kanamycin-A (**1**), amikacin (**2**), and tobramycin (**3**) were purchased from Sigma-Aldrich. Paromamine (**5**) was obtained by methanolysis of the natural antibiotic paromomycin following the procedure described by Bartz et al.[37]

The monoacetyl derivative (**6**) of kanamycin was obtained by employing a methodology previously described by Hanessian and Patil.[30]

The monoacetyl derivative (**7**) of tobramycin was obtained enzymatically, employing the 2-acyl-transferase AAC(2′) from *Mycobacterium tuberculosis*. The plasmid codifying for the AAC(2′)-Ic from *M. tuberculosis* was kindly provided by J. S. Blanchard (Albert Einstein College of Medicine, New York). This plasmid was transformed in the *E. coli* strain BL21(DE3). The expression and purification of *M. tuberculosis* AAC(2′) were performed as described by J. S. Blanchard et al.[38]

The aminoglycoside (2.5 mM) together with the AcCoA (5.0 mM) were dissolved in 5 mM phosphate buffer at pH 7.0. After addition of the enzyme (20 μM), the evolution of the reaction mixture at 303 K was monitored by NMR. The tobramycin derivative was purified by ion exchange column chromatography (0.5 cm × 7 cm) with Amberlite CG-50 (0−7.5% NH_4OH).

Finally, aminoglycoside derivative **8** was prepared from neomycine-B following the procedure described by Chang et al.[34]

DFT Calculations. All calculations were carried out using the B3LYP hybrid functional[39] with the 6-31G(d) basis set. Full geometry optimizations were carried out using the Gaussian 03 package.[40] Analytical frequencies were calculated at the B3LYP/6-31G(d) level to determine the nature of the optimized geometries. BSSE corrections were not considered in this work. Solvent (water) effects were taken into account throughout this study using the polarized continuum model (PCM),[41] as implemented in Gaussian 03. The PCM model accounts for both the electrostatic and the nonelectrostatic components of the solvation energy, including dispersion and cavitation terms, through empirical parameters. The solute molecular cavity was defined through the keyword UAHF.

NMR-Based Conformational Analysis of Derivatives 1−8. NMR experiments were recorded on a Varian Unity 500 and Bruker Avance 500 at 313 K. The spectra of aminoglycosides **1**−**8** were assigned employing a combination of 2-D TOCSY, NOESY, and HSQC experiments.

The TOCSY[42] and NOESY[43] experiments were performed in the phase-sensitive mode with the TPPI method[44] for quadrature detection in F1. Typically, a data matrix of 2000 × 512 points was employed to digitize a spectral width of 4000 Hz. A total of 48 scans was used per increment with a relaxation delay of 1 s. Prior to Fourier transformation, zero filling was performed in F1 to expand the data to 2000 × 2000. Baseline correction was applied in both dimensions. The TOCSY spectra were recorded using MLEV-17[42] during the 60 ms of the isotropic mixing period. The NOESY experiments were performed with mixing times of 400, 800, and 1000 ms.

(37) Haskell, T. H.; French, J. C.; Bartz, Q. R. *J. Am. Chem. Soc.* **1959**, *81*, 3481−3482.
(38) Hegde, S. S.; Javid-Majd, F.; Blanchard, J. S. *J. Biol. Chem.* **2001**, *276*, 45876−45881.
(39) (a) Lee, C.; Yang, W.; Parr, R. *Phys. Rev. B* **1988**, *37*, 785−789. (b) Becke, A. D. *J. Chem. Phys.* **1993**, *98*, 5648−5652.
(40) Pople, J. A. et al. *Gaussian 03*, revision C.01; Gaussian, Inc.: Wallingford, CT, 2004.
(41) (a) Cossi, M.; Barone, V.; Mennucci, B.; Tomasi, J. *Chem. Phys. Lett.* **1998**, *286*, 253−260. (b) Tomasi, J.; Mennucci, B.; Cances, E. *J. Mol. Struct.* **1999**, *464*, 211−226. (c) Cossi, M.; Scalmani, G.; Rega, N.; Barone, V. *J. Chem. Phys.* **2002**, *117*, 43−54.
(42) Bax, A.; Davis, D. G. *J. Magn. Reson.* **1985**, *65*, 355−360.
(43) Kumar, A.; Ernst, R. R.; Wuthrich, K. *Biochem. Biophys. Res. Commun.* **1980**, *95*, 1−6.
(44) Marion, D.; Wuthrich, K. *Biochem. Biophys. Res. Commun.* **1983**, *113*, 967−74.

HSQC experiments were carried out to obtain the complete ^{1}H and ^{13}C assignments. A data matrix of 1000 × 1000 was used to digitize a spectral width of 4000 Hz in F_2 and 15000 Hz in F_1. A total of 32 scans was used per increment with a relaxation delay of 1 s and a delay corresponding to a J value of 145 Hz. ^{13}C decoupling was achieved by the WALTZ scheme.

Selective 1-D NOE experiments were recorded employing the 1-D DPFGSE NOE pulse sequence.[45] NOE intensities were normalized with respect to the diagonal peak at zero mixing time. Selective T_1 measurements were performed on the anomeric and several other protons to obtain the previously mentioned values. Experimental NOEs were fitted to a double exponential function, $f(t) = p0(e^{-p1t})(1 - e^{-p2t})$ with $p0$, $p1$, and $p2$ being adjustable parameters.[46] The initial slope was determined from the first derivative at time $t = 0$, $f'(0) = p0p2$. From the initial slopes, interproton distances were obtained by employing the isolated spin pair approximation.

MD-tar Simulations. To obtain a NMR-derived ensemble, MD-tar[27] simulations were performed for compounds **1**−**8** employing a protocol identical to that described by Asensio et al.[23] RESP atomic charges for **1**−**8** were derived by applying the RESP module of AMBER 5.0 package[28] to the HF/6-31G(d) ESP charges calculated with Gaussian 03.[40] All MD simulations were carried out using the SANDER module within AMBER and the Cornell et al. force field.[47] Parameters for the acetalic functions were taken from GLYCAM.[48] NOE-derived distances were included as time-averaged distance constraints, employing $<r^{-6}>^{-1/6}$ averaging. An exponential decay constant of 8 ns and simulation length of 80 ns were employed. MD-tar trajectories were collected in the absence of explicit solvent but using $\epsilon = 80$ to simulate the water environment.

Unrestrained Molecular Dynamics Simulations. The solute molecule was first immersed in a TIP3P[49] bath of water molecules using the LEAP module of AMBER. The simulation was performed using periodic boundary conditions and the particle-mesh Ewald approach[50] to introduce long-range electrostatic effects. The SHAKE algorithm[51] for hydrogen atoms, which allows using a 2 fs time step, was also employed. Finally, a 9 Å cutoff was applied to Lennard-Jones interactions. Equilibration of the system was carried out as follows: as a first step, a short minimization with positional restraints on solute, by a harmonic potential with a force constant of 500 kcal mol^{-1} Å^{-2}, was done. A 12.5 ps molecular dynamics calculation at 300 K maintaining positional restraints on the solute was then run to equilibrate the water box. For these two steps, a 9 Å cutoff was used for the treatment of the electrostatic interactions. As a next step, the system was equilibrated during an additional 12.5 ps period but now using the mesh Ewald method, as water properties are slightly different with this treatment. Then, the system was subjected to several minimization cycles gradually reducing positional restraints on the solute from 500 to 0 kcal mol^{-1} Å^{-2}. Finally, one unrestrained MD trajectory at constant pressure (1 atm) and temperature (300 K) was collected and analyzed. The simulation length was 5 ns in all cases.

Binding Experiments. The labeled 27-mer A-site model was obtained in its polyacrylamide gel electrophoresis (PAGE) purified sodium salt form, from Dharmacon Research, Inc. (Lafayette, CO). Buffer conditions for the binding experiments were 100 mM NaCl and 10 mM sodium phosphate (pH 7.0). Fluorescence experiments were conducted on a Fluorolog-3 spectrophotometer (Jobin Yvon-Spex Instruments S.A., Inc., Edison, NJ) equipped with a thermostat. A quartz cell with a 1 cm path length in both the excitation and the emission directions was used in all the experiments, which were performed at 298 K. The RNA concentration was, in all cases, 2 μM in strand. For renaturing, RNA was placed in a water bath at 293 K, heated to 358 K for 1 min, and then slowly cooled back to 293 K over a 2 h period. With the excitation wavelength set at 310 nm, the change in the fluorescence emission at 369 nm upon complex formation was followed in the titration experiments. Aliquots of the antibiotic derivatives were added sequentially, and 2 min of equilibration time was allowed before each fluorescence measurement. Fluorescence intensities were corrected for volume changes according to the following equation: $F_{i,\mathrm{corr}} = F_{i,\mathrm{obs}}V_i/V_o$, where $F_{i,\mathrm{corr}}$ is the corrected intensity for point i of the titration, $F_{i,\mathrm{obs}}$ is the measured intensity at point i, V_i is the volume after the ith addition, and V_o is the initial volume (typically, 2 mL). The K_d values for simple binding were determined by plotting $F_{i,\mathrm{corr}}$ against the ligand to RNA ratio. In all cases, the data were found to fit well, assuming a 1:1 complex.

Acknowledgment. We thank Prof. J. Blanchard (Albert Einstein College of Medicine, New York) for supplying the plasmid encoding *Mycobacterium tuberculosis* AAC(2′). Financial support from DGES (Grant CTQ2004-04494) is acknowledged. F.C. thanks the Ministerio de Educación y Ciencia for a *Ramon y Cajal* contract. We also thank CESGA (Santiago de Compostela) for computer support.

Supporting Information Available: Table S1, showing geometrical features calculated at the PCM/B3LYP/6-31G(d) level, for the syn-Ψ and anti-Ψ minima of the model compounds shown in Figure 1. Figures S1−S9, showing details of the NMR experiments and the conformational analysis of the aminoglycosides **1**−**8**. Complete ref 40. This material is available free of charge via that Internet at http://pubs.acs.org.

JA066348X

(45) Stott, K.; Stonehouse, J.; Keeler, J.; Hwang, T. L.; Shaka, A. J. *J. Am. Chem. Soc.* **199**5, *117*, 4199−4200.
(46) Haselhorst, T.; Weimar, T.; Peters, T. *J. Am. Chem. Soc.* **2001**, *123*, 10705−10714.
(47) Cornell, W. D.; Cieplack, P. C.; Bayly, I.; Gould, I. R.; Merz, K.; Ferguson, D. M.; Spellmeyer, D. C.; Fox, T.; Caldwell, J. W.; Kollman, P. A. *J. Am. Chem. Soc.* **1995**, *117*, 5179−5197.
(48) Woods, R. J.; Dwek, R. A.; Edge, C. J.; Fraser-Reid, D. *J. Phys. Chem.* **1995**, *99*, 3832−3839.
(49) Jorgensen, W. L.; Chandrasekhar, J.; Madura, J. D.; Impey, R. W.; Klein, M. L. *J. Chem. Phys.* **1983**, *79*, 926−935.
(50) Sagui, C.; Darden, T. A. *Annu. Rev. Biophys. Biomol. Struct.* **1999**, *28*, 155−179.
(51) Ryckaert, J. P.; Ciccotti, G.; Berendsen, H. J. C. *J. Comput. Phys.* **1977**, *23*, 327−341.